The Function of Toll-like receptor 2 in Infection and Inflammation

Hu, W.

Chapter 3

A novel function of TLR2 and MyD88 in the regulation of leukocyte cell migration behavior during wounding in zebrafish larvae

Wanbin Hu, Leonie van Steijn, Chen Li, Fons J. Verbeek, Lu Cao, Roeland M.H. Merks, Herman P. Spaink

Published in ***Frontiers in cell and developmental biology*** 9 (2021). DOI: 10.3389/fcell.2021.624571

3

Abstract

Toll-like receptor (TLR) signaling via myeloid differentiation factor 88 protein (MyD88) has been indicated to be involved in the response to wounding. It remains unknown whether the putative role of MyD88 in wounding responses is due to a control of leukocyte cell migration. The aim of this study was to explore *in vivo* whether TLR2 and MyD88 are involved in modulating neutrophil and macrophage cell migration behavior upon zebrafish larval tail wounding. Live cell imaging of tail-wounded larvae was performed in *tlr2* and *myd88* mutants and their corresponding wild type siblings. In order to visualize cell migration following tissue damage, we constructed double transgenic lines with fluorescent markers for macrophages and neutrophils in all mutant and sibling zebrafish lines. Three days post fertilization (dpf), tail-wounded larvae were studied using confocal laser scanning microscopy (CLSM) to quantify the number of recruited cells at the wounding area. We found that in both *tlr2*$^{-/-}$ and *myd88*$^{-/-}$ groups the recruited neutrophil and macrophage numbers are decreased compared to their wild type sibling controls. Through analyses of neutrophil and macrophage migration patterns, we demonstrated that both *tlr2* and *myd88* control the migration direction of distant neutrophils upon wounding. Furthermore, in both the *tlr2* and the *myd88* mutants, macrophages migrated more slowly towards the wound edge. Taken together, our findings show that *tlr2* and *myd88* are involved in responses to tail wounding by regulating the behavior and speed of leukocyte migration *in vivo*.

Introduction

Acute inflammation is characterized by the directed migration of leukocytes, which can be triggered by tissue damage [1, 2]. The function of directed leukocyte migration is to eliminate cell debris and invading pathogens, with the aim of maintaining homeostasis upon tissue damage [3]. Neutrophils and macrophages are the two crucial immune cells that engage in this process [2, 4]. Neutrophils are the first cells to rapidly respond to the site of injury, and produce cytokines and chemokines to mediate the recruitment of other cells [4, 5]. However, persisting neutrophil recruitment can release toxic granule contents to further damage tissue, and thereby is a hallmark of chronic inflammatory disease [3, 6, 7]. In comparison, distant macrophages move slower and accumulate later at the wounded area and are considered to play a role in eliminating the debris of apoptotic cells and assist in regeneration of wounded tissue [2, 4, 8, 9]. Leukocyte migration must be tightly regulated to avoid negative effects on tissue repair or further damage. Despite myriad studies on leukocyte migration in response to wounding, the underlying mechanisms are not yet completely understood [10].

Neutrophils and macrophages depend on membrane-localized pattern recognition receptors (PRRs) to sense invading microbes and associated tissue damage [11]. PRRs play a crucial role to recognize pathogen associated molecular patterns (PAMPs) of invading microbes in open wounds and damage associated molecular patterns (DAMPs) released by lysing cells [12, 13]. Toll-like receptors (TLRs) are prominent recognition factors for PAMPs and DAMPs to regulate inflammatory responses [14, 15]. Extensive studies have demonstrated that cellular distribution is different for each TLR. TLRs recognize different classes of PAMPs and trigger the production of cytokines and chemokines during infection. Two typical examples are TLR2, which senses bacterial lipoproteins [16], and TLR4, which recognizes bacterial lipopolysaccharide (LPS) [17]. Accumulating evidence shows that high-mobility group box 1 protein (HMGB1), which is the best well known endogenous danger signal, activates inflammation by forming complexes with other DAMPs (such as single-stranded DNA, nucleosomes and LPS) to be recognized by IL-1R as well as TLR2, TLR4 and TLR9 to induce inflammatory responses [2, 18, 19]. After interacting with these PAMPs and DAMPs, TLRs initiate downstream signaling cascades that ultimately result in producing cytokines and chemokines. Importantly, the activation of downstream signaling pathway by HMGB1 has been shown to be dependent on the TLR down-stream signaling mediated by myeloid differentiation factor 88 protein (MyD88) [2, 20].

TLR2 is one of the best known PRRs and acts as a heterodimer with TLR1 or TLR6 to recognize gram positive bacteria including mycobacteria, presumably based on the specific binding to their cell wall components, such as glycolipids and glycoproteins [16, 21]. TLR2 is expressed and activated after tissue injury even in the absence of infections, like in acute ischemic injury as well as in acute liver and kidney injury [22-25]. In the study of Mojumdar *et al.* (2016), it was shown that macrophage infiltration was reduced into normal muscle following acute injury in TLR2 deficiency mice [26]. In addition, Kim et al. demonstrated that TLR2 contributes to macrophage infiltration in the dorsal root ganglia after peripheral nerve injury in mice [27]. Such injury-induced TLR2 expression and activation has therefore been hypothesized to be important for human health [24, 28, 29]. Following ischemic injury in mice, TLR2 activation promotes cell permeability, lymphocyte invasion and endothelial cell migration and mediates the release of TNF-α and IL-6 [23]. TLR2-deficient mice have a defective ability to recruit neutrophils to an injured liver and fail to induce the neutrophil chemokine CXCL-2 [24]. Additionally, TLR2 contributes to chronic liver disease in a mouse model by mediating MAPK and NF-κB signaling pathways [30]. However, there is little knowledge of the function of Toll-like receptor signaling in cell migration of myeloid cells to epithelial wounding sites [31].

MyD88 is an essential adaptor protein for all TLRs, except TLR3 [32, 33]. MyD88 is responsible for activating downstream signaling through binding to the TIR domain of TLRs [32, 33]. A few studies have shown changes in MyD88 expression after tissue injury. Similar to *Tlr2*, the gene expression of *Myd88* is upregulated following ischemic injury in mice [34]. Moreover, the expression of *Myd88* and *Tlr2* is significantly increased in diabetic wounded mice [35]. In addition, some evidence indicate that Myd88 is involved in the modulation of wound healing [36, 37], but the underlying mechanism is still unclear. Although TLR signaling is important for chemokine production, little is known about the role of MyD88 in leukocyte migratory responses to tissue injuries in the absence of pathogenic infections.

In this paper we use zebrafish larvae as a model for studying leukocyte cell migration after tail wounding. The zebrafish model has become an important vertebrate model for studying human diseases. The small size and transparency of their larvae are useful characteristics for the screening and imaging of transgenic reporter lines [38]. Zebrafish larvae are a popular model for studying functions involved in wound repair [39-44]. The availability of mutants in Toll-like receptor signaling genes *tlr2* and *myd88* make it possible to study their roles in leukocyte migratory behavior upon tail wounding in zebrafish [41, 42, 45-47]. Tlr2 and Myd88 show a

highly conserved structure in mammals and zebrafish [48]. In a previous study, we demonstrated the conserved role of *tlr2* in zebrafish as a PRR to recognize the mammalian TLR2 ligand Pam3CSK4, and identified a set of genes that are specifically expressed genes by activation of the downstream pathway of zebrafish *tlr2* [49]. Moreover, He et al., confirmed that *tlr2* gene expression can be upregulated upon wounding in zebrafish larvae which is consistent with previous studies in mice [50]. In addition, the study of Sommer et al., suggests that *myd88* is required for induction of chemokine gene expression, such as *ccl2* and *cxcl11aa,* following tail wounding [51].

In the present study, live fluorescent imaging was used to investigate the effect of the *tlr2* mutation and the *myd88* mutation on leukocyte migration upon tail wounding. We found reduced numbers of recruited neutrophils and macrophages at the wounding area in both *tlr2* mutants and *myd88* mutants, compared to their sibling controls. Leukocyte migration of the *tlr2* and *myd88* mutations upon wounding was analyzed using quantitative analyses of cell migration tracks. Our results demonstrate that the *tlr2* and the *myd88* mutations affect distant neutrophil migration upon wounding by negatively affecting their directional persistence, but not their migration speed. Not only the directional persistence of distant macrophage was significantly decreased in the *tlr2* and the *myd88* mutants, but also their migration speed. This study shows for the first time that TLR signaling is directly involved in controlling behavior of cell migration of neutrophils and macrophages during wounding, stimulating further studies also in other model systems.

Results

Tlr2 and myd88 mutations do not affect development and basal motility of leukocytes.

To determine the leukocyte development in *tlr2* and *myd88* mutants, the double-transgenic line *tlr2*$^{+/+}$ *Tg (mpeg1:mCherry-F);TgBAC (mpx: EGFP)*, *tlr2*$^{-/-}$ *Tg (mpeg1:mCherry-F);TgBAC (mpx: EGFP), myd88*$^{+/+}$ *Tg (mpeg1:mCherry-F);TgBAC (mpx: EGFP)* and *myd88*$^{-/-}$ *Tg (mpeg1:mCherry-F);TgBAC (mpx: EGFP)* were constructed. The lines were imaged at 3 dpf to count the number of macrophages and neutrophils in their tail region, and then compared with their wild type siblings (Fig. 1A). Embryos of the *tlr2* and *myd88* mutants showed similar numbers of macrophages and neutrophils as their wild type siblings (Fig. 1B- E). This result is consistent with our previous studies of the same *myd88* mutant at 3 dpf and the *tlr2* mutant at 2

dpf [45, 47]. With the aim of investigating the importance of the *tlr2* and the *myd88* mutations for leukocyte behavior under unchallenged condition, the CHT region was analyzed in the double transgenic lines of *tlr2* and *myd8*8 using CLSM by taking time-lapse images (Fig. 1A). No significant effect was observed on leukocyte basal motility in the CHT tissue in the *tlr2* and *myd88* mutants compared with their wild type sibling control (Fig. 1F-M). Representative images are shown in Fig. S2, 3.

Tlr2 and myd88 regulate neutrophil recruitment to a tail wound

To study the effect of the *tlr2* and *myd88* mutations on the recruitment of neutrophils towards a site of injury, a tail wound method was used in 3 dpf zebrafish larvae as a model for inflammation. To quantify the number of recruited neutrophils to the wound, we counted the number of neutrophils that were located in a range closer than 200 μm from the wound edge of the tail at 1, 2, 4 and 6 hpw (Fig. 2A). Our results show that the *tlr2* mutation had a significant negative effect on the recruitment of neutrophils after 2, 4 and 6 hpw (Fig. 2B, C). However, there is no significant difference in recruited neutrophil numbers between wild type and *tlr2*$^{-/-}$ at 1 hpw (Fig. 2B, C). Notably, a significant difference of recruited neutrophil numbers was already observed at 1 hpw in *myd88* zebrafish larvae and remained significant until 6 hpw (Fig. 2D, E).

Tlr2 and myd88 regulate macrophage recruitment to a tail wound

To assess the role of the *tlr2* and *myd88* mutations in regulating the recruitment of macrophages to a site of the tail wound, we counted the recruited macrophage numbers by the same method as for measuring the neutrophil recruitment to the wound (Fig. 3A). Both *tlr2*$^{-/-}$ and *myd88*$^{-/-}$ mutant zebrafish larvae displayed diminished macrophage responses upon wounding (Fig. 3). Significantly decreased numbers of recruited macrophages toward the injury were measured in the *tlr2*$^{-/-}$ group at 2, 4 and 6 hpw (Fig. 3B, C). Similarly, there is no significant difference in recruited macrophage numbers between wild type and *tlr2*$^{-/-}$ at 1 hpw (Fig. 3C). A significant difference of recruited macrophage numbers was already observed from 1 hpw in *myd88* zebrafish larvae, the same as was observed with neutrophil recruitment (Fig. 3D ,E).

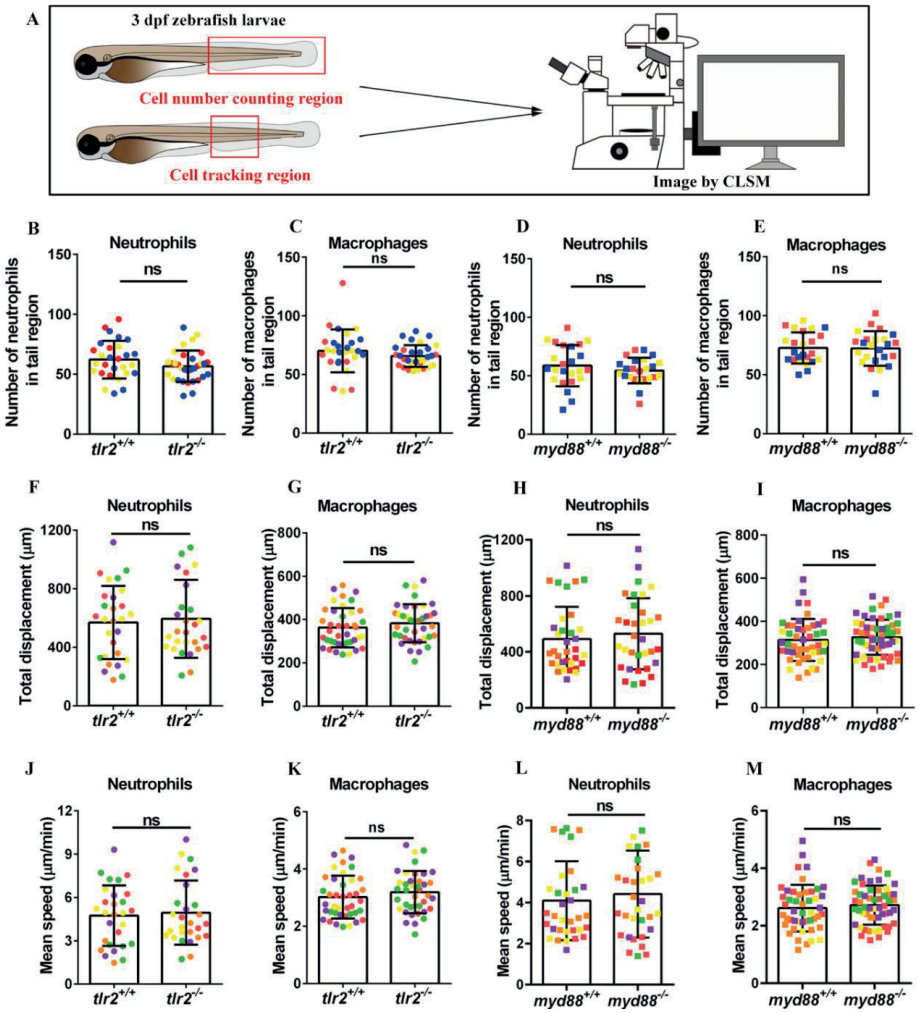

Figure 1 Quantification of macrophage and neutrophil numbers and their basal migratory capability in the 3 dpf *tlr2 and myd88* mutants and wild sibling controls larvae. (A) Experimental scheme. At 3 dpf, numbers and basal migratory capability of GFP-labeled neutrophils and mCherry-labeled macrophages in tail region were quantified using Leica TCS SP8 confocal laser scanning microscopy (CLSM). Red boxes show the area in which cells were counted or tracked. (B- E) The quantification of neutrophil and macrophage numbers in tail region by using *tlr2* and *myd88* zebrafish larvae. Data (mean ± SD) are combined from three pools of zebrafish larvae. No significant differences (ns) in the number of neutrophils (B, D) and macrophages (C, E) was detected with an unpaired, two-tailed t-test. Each point represents one larva and different colors represent different pools. Sample size (n): 28, 32 (B, C); 24, 24 (D, E). (F- G, J- K) Quantification of basal migratory capability in 3 dpf *tlr2* zebrafish. The total displacement and mean speed of individual neutrophils (F, J) and macrophages (G, K) were quantified by using a manual tracking plugin. Data (mean ± SD) are combined from 5 larvae of *tlr2*$^{+/+}$ *Tg (mpeg1:mCherry-F);TgBAC (mpx: EGFP)* and *tlr2*$^{-/-}$ *Tg (mpeg1:mCherry-F);TgBAC (mpx: EGFP)* larvae respectively. Each color indicates a different larva. No significant differences (ns) in the total displacement and mean speed of neutrophils (F, J) and macrophages (G, K) were detected with an unpaired, two-tailed t-test. Sample size (n): 28, 28 (F, J); 40, 39 (G, K). Cell tracking movies are shown in Supplementary Movie S1-4). (H- I, L- M) Quantification of basal migratory capability in 3 dpf *myd88* zebrafish. The total displacement and mean speed of individual neutrophils (H, L) and macrophages (I, M) were quantified by using a manual tracking plugin. Data (mean ± SD) are combined from 5 larvae of *myd88*$^{+/+}$ *Tg (mpeg1:mCherry-F);TgBAC (mpx: EGFP)* and *myd88*$^{-/-}$ *Tg (mpeg1:mCherry-F);TgBAC (mpx: EGFP)* larvae respectively. Each color indicates a different larva. No significant differences (ns) in the total displacement and mean speed of neutrophils (H, L) and macrophages (I, M) were detected with an unpaired, two-tailed t-test. Sample size (n): 34, 33 (H, L); 47, 55 (I, M). Cell tracking movies are shown in Supplementary Movie S5-8).

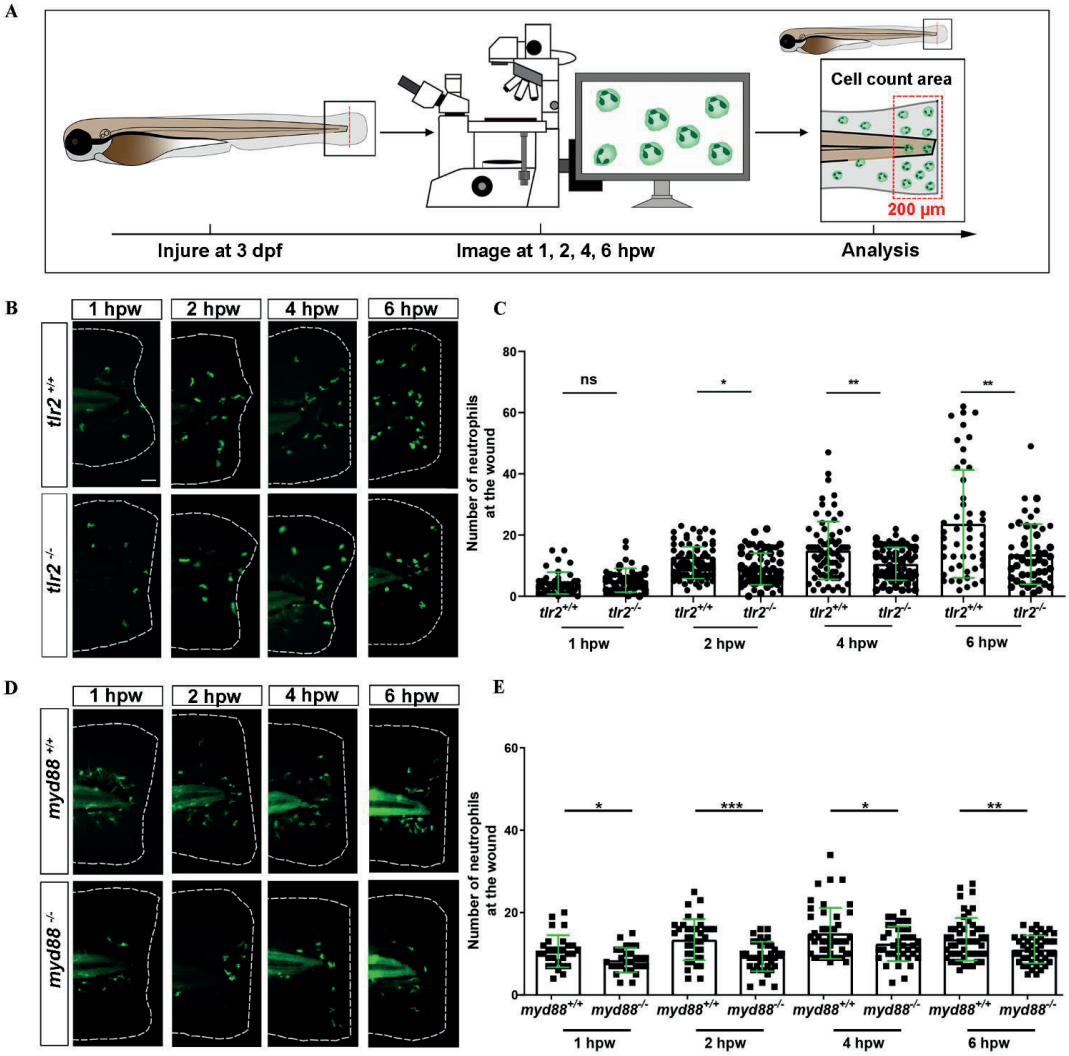

Figure 2 The number of neutrophils recruited to the wounded area in the *tlr2* and *myd88* mutants and wild type sibling controls larvae. (A) Experimental scheme. *Tlr2* and *myd88* homozygous mutants and sibling control larvae were wounded at 3 dpf. Their tails were wounded to the tip of the notochord. The red dashed line shows the site of wounding. Recruited neutrophils at the wound were imaged at 1, 2, 4 and 6 hpw by using CLSM. For recruited cell counting analysis, cells localized within an area of 200 µm from the wounding edge toward the body trunk were counted as recruited cells. The red dashed box shows the area where neutrophils were counted as recruited neutrophils. (B, D) Representative images of 3 dpf larvae at 1, 2, 4 and 6 hours post-wounding (hpw). Scale bar: 50 µm. (C) Quantification of recruited neutrophil numbers to the wounded area at 1, 2, 4 and 6 hpw in 3 dpf *tlr2*$^{+/+}$ and *tlr2*$^{-/-}$ larvae. Each point represents a different larva. Sample size (n): 45, 46, 82, 72, 74, 68, 50, 50. (E) Quantification of recruited neutrophil numbers to the wounded area at 1, 2, 4 and 6 hpw in 3 dpf *myd88*$^{+/+}$ and *myd88*$^{-/-}$ larvae. Each point represents a different larva. Sample size (n): 29, 28, 37, 38, 45, 39, 51, 45. In all cases, statistical analyses were done from 3 independent experiments. An unpaired, two-tailed t-test was used to assess significance (ns, no significant difference, *$P < 0.05$, **$P < 0.01$, ***$P < 0.001$) and data are shown as mean± SD.

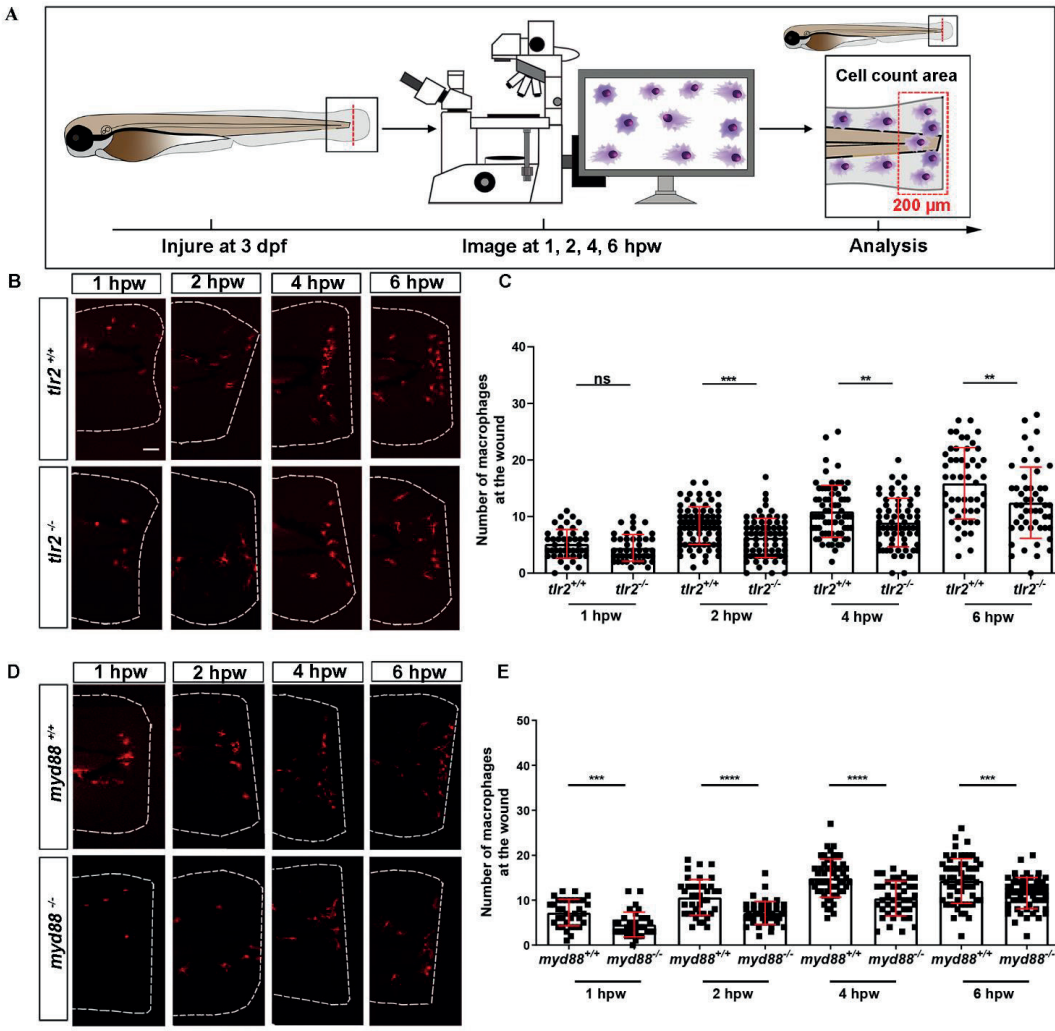

Figure 3 The number of macrophages recruited to the wounded area in the *tlr2* and *myd88* mutants and wild type sibling controls larvae. (A) Experimental scheme. *Tlr2* and *myd88* homozygous mutants and sibling control larvae were wounded at 3 dpf. Their tails were wounded to the tip of the notochord. The red dashed line shows the site of wounding. Recruited macrophages at the wound were imaged at 1, 2, 4 and 6 hpw by using CLSM. For recruited cell counting analysis, cells localized within an area of 200 µm from the wounding edge toward the body trunk were counted as recruited cells. The red dashed box shows the area where macrophages were counted as recruited macrophages. (B, D) Representative images of 3 dpf larvae at 1, 2, 4 and 6 hpw. Scale bar: 50 µm. (C) The quantification of recruited macrophage numbers to the wounded area at 1, 2, 4 and 6 hpw in 3 dpf $tlr2^{+/+}$ and $tlr2^{-/-}$ larvae. Each point represents a different larva. Sample size (n): 45, 45, 82, 71, 69, 68, 51, 50. (E) The quantification of recruited macrophage numbers to the wounded area at 1, 2, 4 and 6 hpw in 3 dpf $myd88^{+/+}$ and $myd88^{-/-}$ larvae. Each point represents a different larva. Sample size (n): 35, 34, 40, 43, 56, 42, 60, 58. In all cases, statistical analyses were done with data of 3 independent experiments. An unpaired, two-tailed t-test was used to assess significance (ns, no significant difference, $^{**}P < 0.01$, $^{***}P < 0.001$, $^{****}P < 0.0001$) and data are shown as mean± SD.

Live imaging reveals that the *tlr2* and *myd88* mutations affect distant neutrophil directional persistence, but not migration speed upon tail wounding

To investigate how neutrophils migrate in the absence of *tlr2* or *myd88* after tail wounding, a time-lapse microscopy experiment was performed by using CLSM between 1 hpw to 3 hpw (Fig. 5, 6). The definition of distant and local resident neutrophils was shown in panel A of Fig. 5-6 and Fig. S4-5. Neutrophils located closer than 200μm to the wound were defined as local resident neutrophils and further than 200μm were defined as distant neutrophils. Measurement of the distance to the wound over time of all distant neutrophils in the *tlr2*$^{-/-}$ group indicated a trend of impaired infiltration towards the wound (Fig. 5B,C up panel). In total, the group of distant neutrophils in the *tlr2*$^{+/+}$ group that arrived at the wound edge and stayed within a distance of 20 μm to the wound comprises 84 % of a total of 25 tracked neutrophils (Fig. 5C up panel). The local resident neutrophils in this group all remained at the wound (Fig. S4B, C up panel). In contrast, the group of the distant neutrophils in the *tlr2*$^{-/-}$ group that arrived at the wound within 2 h time-lapse cell tracking comprises only approximately 36 % (Fig. 5B,C bottom panel). Moreover, approximately 33 % of local resident neutrophils in the *tlr2*$^{-/-}$ group already migrated away from the wound edge within 3 hpw (Fig. S4B,C bottom panel).

In general, distant neutrophils in the *myd88*$^{+/+}$ group showed more chemotaxis to the wound compared to *myd88*$^{-/-}$ neutrophils (Fig. 6B,C). Approximately 96.7% distant neutrophils arrived at the wound (within a distance of 20 μm to the wound) in the *myd88*$^{+/+}$ group in total (Fig. 6C up panel). However, only 86.4% distant neutrophils arrived to the wound (within a distance of 20 μm to the wound) in the *myd88*$^{-/-}$ group. (Fig. 6C bottom panel). The local resident neutrophils in this group all remained at the wound except for a few outliers (Fig S5C). In summary, the general trend of distant neutrophils migration in the *myd88* mutant and sibling zebrafish groups was consistent with the result in the *tlr2* mutant and sibling zebrafish groups, respectively (Fig 6C).

To quantify differences in neutrophil migration behavior between *tlr2* and *myd88* mutants and their wild type siblings, we first analyzed whether the deficiency of *tlr2* and *myd88* can affect neutrophil mean migration speed upon wounding. The results showed that the *tlr2* and the *myd88* mutations do not affect the mean speed of both distant and local resident neutrophils upon the wounding (Fig. 5D; Fig. 6D; Fig. S4D and Fig. S5D). In addition to manual cell tracking analysis we also performed automatic 3D cell tracking by using a Viterbi Algorithm [52]. The results, shown in Fig. S8, confirm that there is no difference in mean speed between

mutant and sibling neutrophils. However, automatic tracking of living cells showed to be very challenging due to the complex leukocyte cell behaviors. Since in the automated method there are cell disappearing and appearing leading to gaps in the time series images it is currently still outperformed by manual tracking.

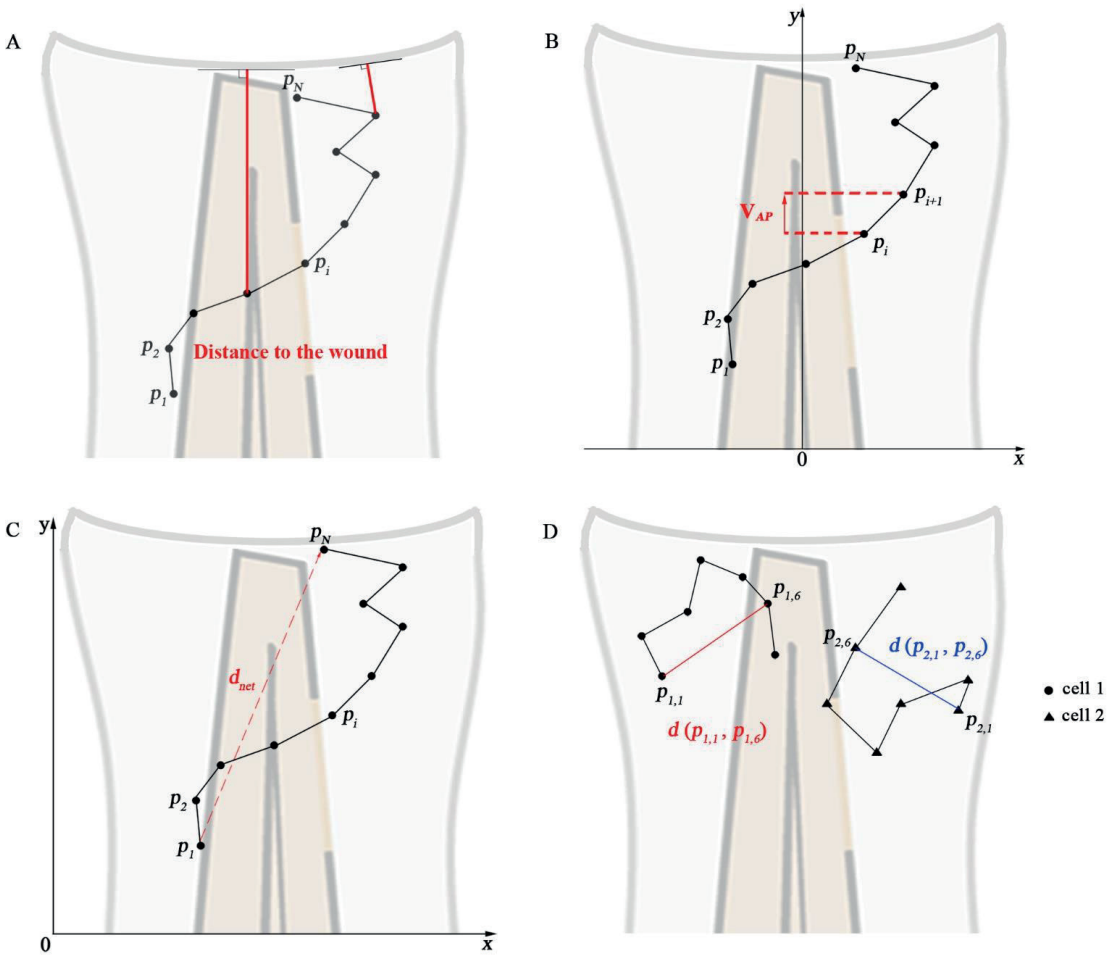

Figure 4 Calculated track measures.
(A) Depiction of distance to the wound. It measured for each frame as the shortest distance from the cell's current position to the entire line of the wound, i.e. the orthogonal projection to the wound.
(B) Depiction of V_{AP}: velocity in anteroposterior axis direction. The visible part of the spine is taken as the y-axis.
(C) Depiction of the net displacement, total displacement, meandering index and mean speed: the net displacement is the distance of the cell between the first and final time frame. Total displacement is the sum of the net displacement between 2 successive frames. Meandering index corresponds to the net displacement divided by the total displacement. Mean speed is the total displacement divided by traveled time. Formulas show in Table 1. (Eq. 1-4).
(D) Depiction of the construction of the mean squared displacement: the displacement between the first time frame and time frame t from all cells is squared and averaged, see Table 1. (Eq. 5).

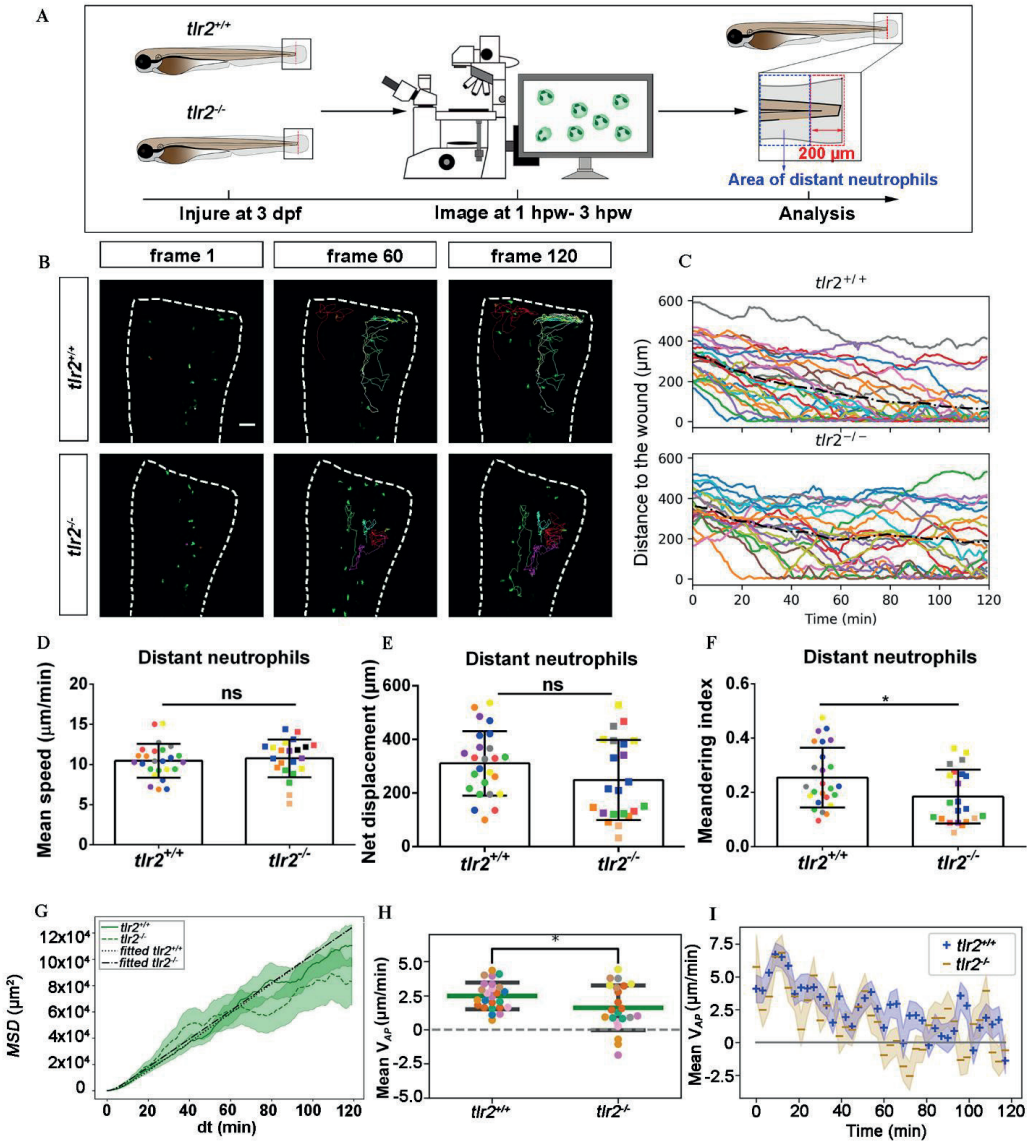

Figure 5 Quantification of distant neutrophils behavior in wounded *tlr2* mutant and sibling control larvae. (A) Experimental scheme. *Tlr2*$^{+/+}$ and *tlr2*$^{-/-}$ larvae were wounded at 3 dpf. The red dashed line shows the site of wounding. Neutrophils of wounded zebrafish larvae were tracked for 2 h and images were taken every 1 min by using CLSM. For cell tracking analysis, cells localized outside an area of 200 µm from the wounding edge toward the body trunk were counted as distant cells. Blue dashed box shows the area where distant neutrophils were tracked. (B) Representative images of distant neutrophil tracks in the wounded tail fin of 3 dpf *tlr2*$^{+/+}$ or *tlr2*$^{-/-}$ larvae at frame 1, frame 60 and frame 120. Time interval between two successive frames is 1 min. Each color track represents an individual neutrophil. Cell tracking movies are shown in Supplementary Movie S9-10). Scale bar: 50 µm. (C) Distance to the wound. Black dash line represents average distance to the wound. Each color line represents one cell. (D-I) Quantification of distant neutrophil tracks. In panel D-F and H, each color indicates a different larva. There was no significant difference between the groups in terms of mean speed (D), net displacement (E) and MSD (green) and fitted MSD (black) (G). However, meandering index (F) and mean V_{AP} (H) of neutrophils at the wound in *tlr2*$^{+/+}$ is greater than in *tlr2*$^{-/-}$ larvae. The fitted MSD (G, black) was fitted for $dt < 80$ min. The shaded regions in MSD (G) and mean V_{AP} over time (I) indicate standard error of the mean. Statistical analyses were done with 7 and 8 fish respectively for each group. An unpaired, two-tailed t-test was used to assess significance (ns, non-significance, $*P < 0.05$) and data are shown as mean± SD. Sample size (n): 25, 22 (D, E, F, H).

We also tested the effect of the *tlr2* and the *myd88* mutations on the movement direction of neutrophils upon wounding by the quantification of net displacement, whose definition is shown in Fig. 4 and Table 1. We observed that the net displacement of distant neutrophils had a decreased trend in the $tlr2^{-/-}$ group compared to the $tlr2^{+/+}$ group (Fig. 5E). Moreover, cell diffusivity determined by the fitting Eq. 6 to the MSD curve (Table 1.) did not differ much between the $tlr2^{-/-}$ group (277 μm^2/min) and the $tlr2^{+/+}$ group (268 μm^2/min) (Fig. 5G). A significant decrease in net displacements was consistently observed in the *myd88* mutant group (Fig. 6E). Also, $myd88^{-/-}$ neutrophils have lower diffusivity (274 μm^2/min) than $myd88^{+/+}$ neutrophils (412 μm^2/min) as measured from the slopes of the MSD plots (Fig. 6G). As the cell speed of $myd88^{-/-}$ neutrophils does not differ from that of $myd88^{+/+}$ neutrophils (Fig. 6D), the reduced diffusivity may be due to more frequent or sharper changes of direction of the $myd88^{-/-}$ neutrophils. As neutrophils reach the wound edge, their diffusivity is limited in space. This is also visible in the flattening of the MSD at later time frames. Hence, fitting Eq. 6 to the MSD curve was limited to $dt < 80$.

To further study the effect of the *tlr2* and *myd88* mutations on the neutrophil migration direction, we determined the meandering index and mean V_{AP} (Fig. 5F,H and Fig. 6F,H). The meandering index and mean V_{AP} are all significantly decreased in the distant neutrophils of both $tlr2^{-/-}$ and $myd88^{-/-}$ mutants compared to their wild type sibling controls (Fig. 5F,H and Fig. 6F,H). However, no significant difference of meandering index was found in local resident neutrophils of the $tlr2^{-/-}$ and $myd88^{-/-}$ mutants compared to the wild type siblings (Fig. S4F and Fig. S5F). The mean V_{AP} over time qualitatively shows again the impaired chemotaxis of $tlr2^{-/-}$ and $myd88^{-/-}$ neutrophils compared to the $tlr2^{+/+}$ and $myd88^{+/+}$ neutrophils, respectively (Fig. 5I and Fig. 6I). As more and more neutrophils approach the wound (Fig. 5C, 6C), the mean V_{AP} drops. For almost every time point, mean V_{AP} of $tlr2^{+/+}$ exceeds mean V_{AP} of $tlr2^{-/-}$ (Fig. 5I). Similar results were observed for $myd88^{+/+}$ and $myd88^{-/-}$ distant neutrophils (Fig. 6I).

Live imaging reveals that the *tlr2* and *myd88* mutations affect distant macrophage migration speed and directional persistence upon tail wounding

To study the effect of the *tlr2* and *myd88* mutations on macrophage migration upon wounding, we compared macrophage behavior with their wild type siblings. The definition of distant macrophage and local resident macrophage was shown in panel A of Fig. 7-8 and Fig. S6-7. Macrophages located closer than 200μm to the wound were defined as local resident

macrophages and further than 200μm were defined as distant macrophages. In contrast to neutrophils, the majority of macrophages do not reach the wound within the measured time period. By measuring their distance to the wound over time, we can see a trend that distant macrophages show less chemotaxis in the *tlr2*$^{-/-}$ and *myd88*$^{-/-}$ mutant groups compared to their wild type sibling groups (Fig. 7 B, C and Fig. 8B, C). Within 50 μm to the wound, the local resident macrophages all remained at the wound in both the *tlr2* and *myd88* mutants and their wild type sibling controls (Fig. S6B, C and Fig. S7B, C). Within a distance of 200 μm, but outside 50 μm to the wound, local resident macrophages tend to migrate to the wound direction (Fig. S6B, C and Fig. S7B, C).

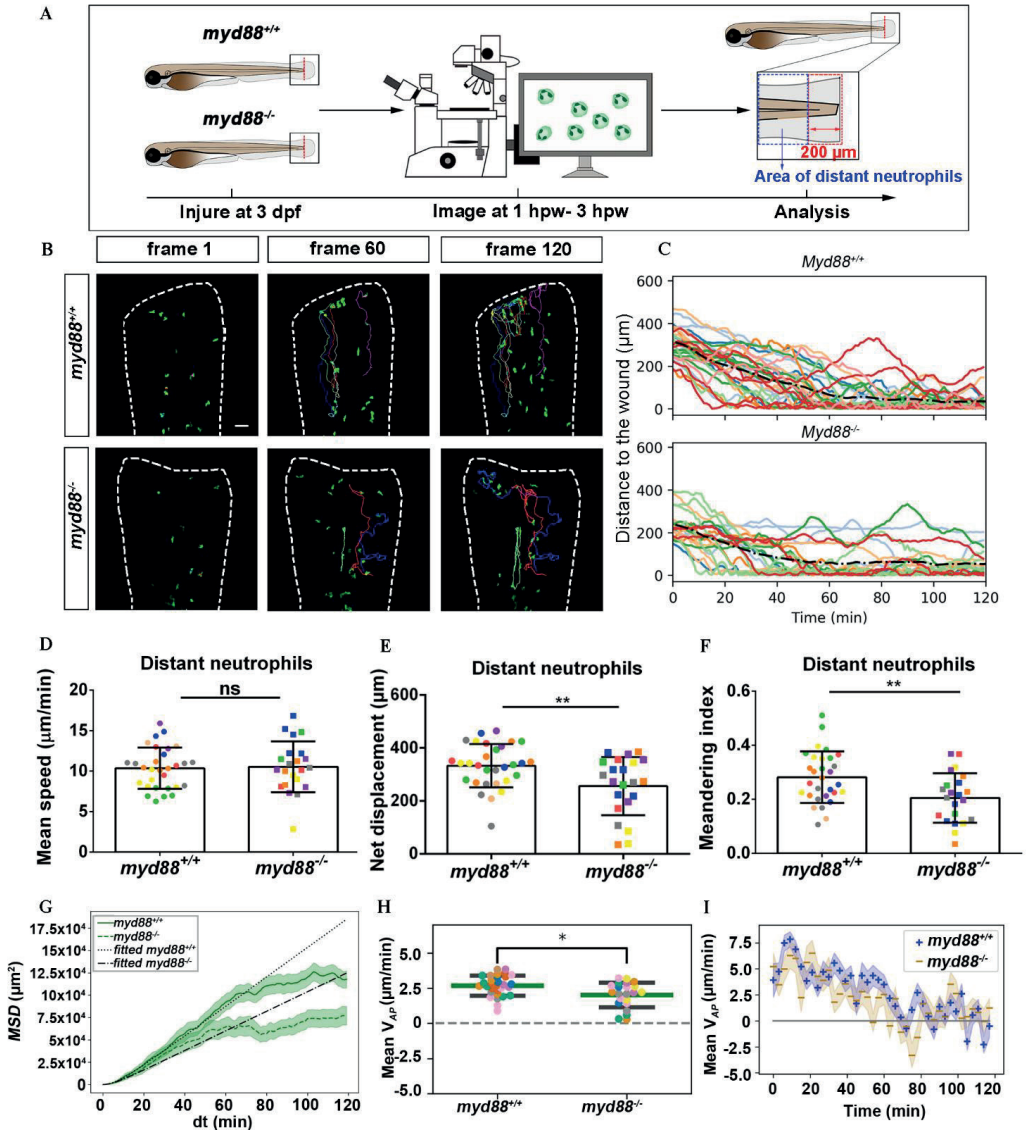

Figure 6 Quantification of distant neutrophils behavior in wounded *myd88* mutant and sibling control larvae. (A) Experimental scheme. *Myd88*$^{+/+}$ and *myd88*$^{-/-}$ larvae were wounded at 3 dpf. The red dashed line shows the site of wounding. Neutrophils of wounded *myd88* zebrafish larvae were tracked for 2 h and images were taken every 1 min by using CLSM. For cell tracking analysis, cells localized outside an area of 200 µm from the wounding edge toward the body trunk were counted as distant cells. Blue dashed box shows the area where distant neutrophils were tracked. (B) Representative images of distant neutrophil tracks in the wounded tail fin of 3 dpf *myd88*$^{+/+}$ or *myd88*$^{-/-}$ larvae at frame 1, frame 60 and frame 120. Time interval between two successive frames is 1 min. Each color track represents an individual neutrophil. Cell tracking movies are shown in Supplementary Movie S11-12). Scale bar: 50 µm. (C) Distance to the wound. Black dash line represents average distance to the wound. Each color line represents one cell. (D-I) Quantification of distant neutrophil tracks. In panel D-F and H, each color indicates a different larva. There was no significant difference between the groups in terms of mean speed (D). However, the net displacement (E), meandering index (F),), MSD (green) and fitted MSD (black) (G) and mean V_{AP} (H) of neutrophils at the wound in *myd88*$^{+/+}$ is greater than in *myd88*$^{-/-}$ larvae. The shaded regions MSD (G) and in mean V_{AP} over time (I) indicate standard error of the mean. The fitted MSD (G, black) was fitted for $dt < 80$ min. Statistical analyses were done with 8 and 7 fish respectively for each group. An unpaired, two-tailed t-test was used to assess significance (ns, non-significance, $^{**}P < 0.01$) and data are shown as mean± SD. Sample size (n): 30, 22 (D, E, F, H).

To quantify differences in macrophage migration behavior between *tlr2* and *myd88* mutants and their wild type siblings, we first analyzed whether the deficiency of *tlr2* and *myd88* can affect macrophage mean migration speed upon wounding. Following tail wounding, both distant and local resident macrophages migrate more slowly in the $tlr2^{-/-}$ and $myd88^{-/-}$ mutant groups than in the wild type sibling controls (Fig. 7D; Fig. 8D; Fig. S6D; Fig. S7D). In addition to manual cell tracking analysis we also performed automatic cell tracking by using a Viterbi Algorithm [52] (Fig. S8). The results from this automated 3D cell tracking confirm the significant difference in mean speed between mutant and sibling macrophages (Fig. S8).

Subsequently, we studied the directional persistence of macrophage migration upon wounding. To this end, we quantified the net displacement, meandering index and mean V_{AP} in the *tlr2* and *myd88* mutants and siblings. The net displacement of the distant macrophages (Table 1. Eq. 1) was reduced in the $tlr2^{-/-}$ and $myd88^{-/-}$ mutants compared to the controls (Fig. 7E; Fig. 8E). The meandering index (Table 1. Eq. 3) and mean V_{AP} of distant macrophages were also significantly decreased in the $tlr2^{-/-}$ and $myd88^{-/-}$ groups (Fig. 7F,H and Fig. 8F,H). However, no significant differences in net displacement were found in local resident *tlr2* and *myd88* macrophage groups (Fig. S6E and Fig. S7E). The trend of mean V_{AP} over time is similar to the one observed for distant neutrophils, in that $tlr2^{+/+}$ and $myd88^{+/+}$ macrophages have a higher mean V_{AP} than $tlr2^{-/-}$ and $myd88^{-/-}$ macrophages during the entire tracking period. The mean V_{AP} of macrophages is positive for a longer period of time compared to the neutrophils, as the majority of macrophages have not reached the wound site during the 2h time span.

The differences in speed and directionality also became apparent from the differences in MSD between the $tlr2^{+/+}$ and $myd88^{+/+}$ distant macrophages versus the $tlr2^{-/-}$ and $myd88^{-/-}$ distant macrophages (Fig. 7G,8G). The MSD (Table 1. Eq. 5) is lower for the $tlr2^{-/-}$ and $myd88^{-/-}$ macrophages, which can reflect a speed reduction and/or a lowered directional persistence. A decreased directional persistence can also be seen through the shape of the MSD curve. For $tlr2^{+/+}$ and $myd88^{+/+}$ distant macrophages, the MSD curve, especially at short time intervals dt, has a parabolic shape, indicating straight cell trajectories. For $tlr2^{-/-}$ and $myd88^{-/-}$, however, the MSD curve has a more linear shape, indicating random cell motility. Finally, the cell diffusivity D is also decreased in the $tlr2^{-/-}$ (38 μm^2/min) and $myd88^{-/-}$ (221 μm^2/min) macrophage groups compared to the $tlr2^{+/+}$ (132 μm^2/min) and $myd88^{+/+}$ (284 μm^2/min) macrophage groups. In summary, the data show that both *tlr2* and *myd88* mutations affect distant macrophage migration speed and directional persistence upon tail wounding.

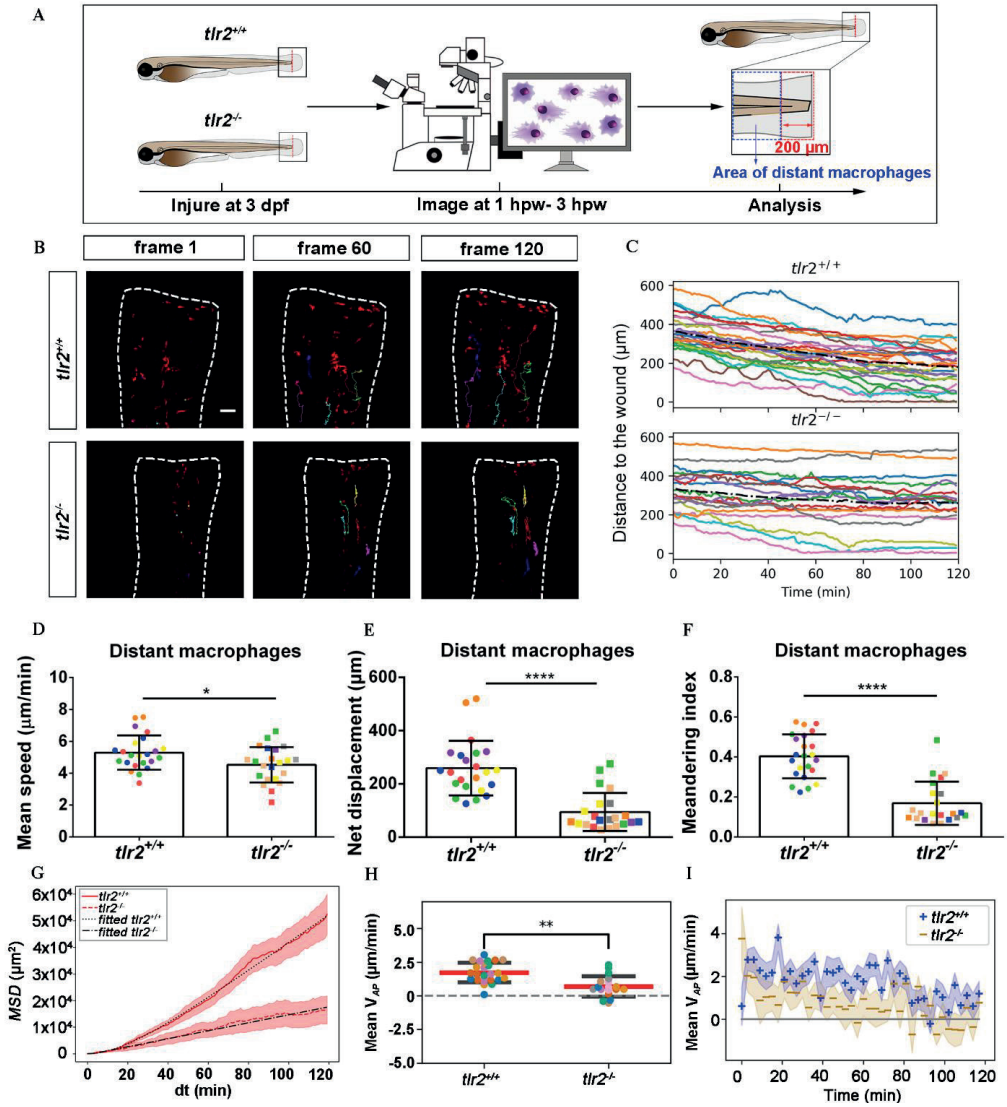

Figure 7 Quantification of distant macrophage behavior in wounded *tlr2* mutant and sibling control larvae. (A) Experimental scheme. *Tlr2*$^{+/+}$ and *tlr2*$^{-/-}$ larvae were wounded at 3 dpf. The red dashed line shows the site of wounding. Macrophages of wounded *tlr2* zebrafish larvae were tracked for 2 h and images were taken every 1 min by using CLSM. For cell tracking analysis, cells localized outside an area of 200 µm from the wounding edge toward the body trunk were counted as distant cells. Blue dashed box shows the area where distant macrophages were tracked. (B) Representative images of distant macrophage tracks in the wounded tail fin of 3 dpf *tlr2*$^{+/+}$ or *tlr2*$^{-/-}$ larvae at frame 1, frame 60 and frame 120. Time interval between two successive frames is 1 min. Each color track represents an individual macrophage. Cell tracking movies are shown in Supplementary Movie S13-14). Scale bar: 50 µm. (C) Distance to the wound. Black dash line represents average distance to the wound. Each color line represents one cell. (D-I) Quantification of distant macrophage tracks. In panel D-F and H, each color indicates a different larva. There was a significant difference between the groups in terms of mean speed (D), net displacement (E), meandering index (F),), MSD (red) and fitted MSD (black) (G) and mean V_{AP} (H) of macrophages. The shaded regions in MSD (G) and mean V_{AP} over time (I) indicate standard error of the mean. Statistical analyses were done with 6 and 8 fish respectively for each group. An unpaired, two-tailed t-test was used to assess significance (ns, non-significance, $*P < 0.05$, $**P < 0.01$, $****P < 0.0001$) and data are shown as mean± SD. Sample size (n): 23, 22 (D, E, F, H).

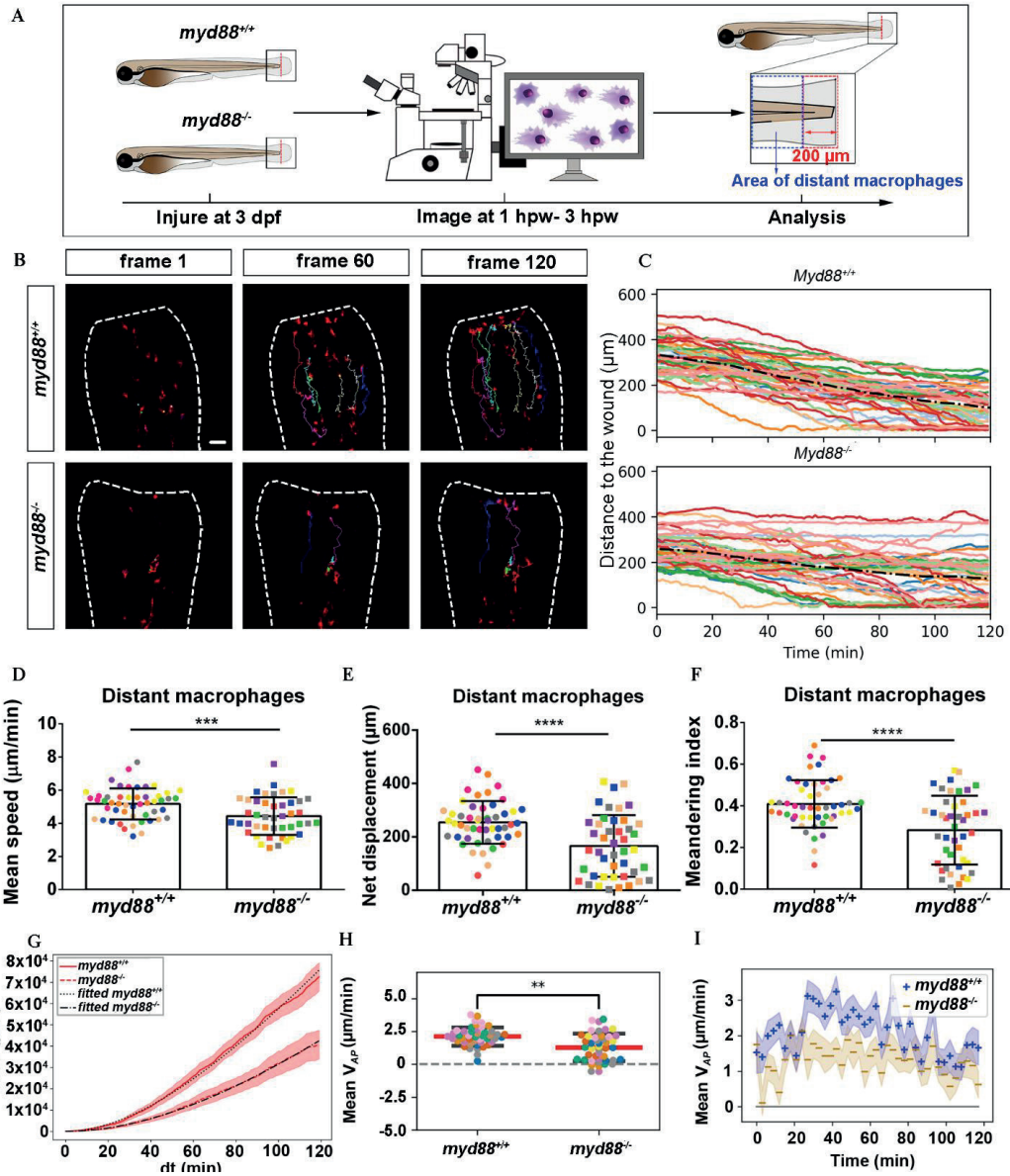

Figure 8 Quantification of distant macrophages behavior in wounded *myd88* mutant and sibling control larvae. (A) Experimental scheme. *Myd88*$^{+/+}$ and *myd88*$^{-/-}$ larvae were wounded at 3 dpf. The red dashed line shows the site of wounding. Macrophages of wounded zebrafish larvae were tracked for 2 h and images were taken every 1 min by using CLSM. For cell tracking analysis, cells localized outside an area of 200 µm from the wounding edge toward the body trunk were counted as distant cells. Blue dashed box shows the area where distant macrophages were tracked. (B) Representative images of distant macrophage tracks in the wounded tail fin of 3 dpf *myd88*$^{+/+}$ or *myd88*$^{-/-}$ larvae at frame 1, frame 60 and frame 120. Time interval between two successive frames is 1 min. Each color track represents an individual macrophage. Cell tracking movies are shown in Supplementary Movie S15-16). Scale bar: 50 µm. (C) Distance to the wound. Black dash line represents average distance to the wound. Each color line represents one cell. (D-I) Quantification of distant macrophage tracks. In panel D-F and H, each color indicates a different larva. There was a significant difference between the groups in terms of mean speed (D), net displacement (E), meandering index (F), MSD (red) and fitted MSD (black) (G) and mean V_{AP} (H) of macrophages. Statistical analyses were done with 9 and 8 fish respectively for each group. The shaded regions in MSD (G) and mean V_{AP} over time (I) indicate standard error of the mean. An unpaired, two-tailed t-test was used to assess significance (ns, non-significance, $*P < 0.05$, $**P < 0.01$, $****P < 0.0001$) and data are shown as mean± SD. Sample size (n): 50, 44 (D, E, F, H).

Discussion

In this study we visualized cell migration in *tlr2* and *myd88* mutants using live-imaging in a zebrafish tail wounding model. Thereby we demonstrated that these genes play a crucial role to control the migration of both neutrophils and macrophages upon tissue wounding. Like in mammals, neutrophils and macrophages play a dominant role in the wounding response during the first several hours after zebrafish tail fin wounding [4, 42, 53]. In mice, it has been shown previously that TLR signaling plays a role in controlling infiltration of neutrophils and macrophages into injured tissue [22-25]. The function of TLR signaling in migration to epithelial wounds has only been studied so far in zebrafish larvae [31]. This study found that knock-down of *myd88* by morpholinos impairs the infiltration of neutrophils into the wound area, but the mechanisms underlying such reduced wound infiltration remained unknown. By using double transgenic lines, here we show that *tlr2* and *myd88* are both essential for directed migration of distant neutrophils and macrophages to the wounded tissue. The meandering index (Fig. 4 and Table 1. Eq. 3) of distant neutrophils and macrophages was significantly decreased in *tlr2* and *myd88* mutant larvae compared with wild type sibling control groups (Fig. 5F, 6F, 7F and 8F). Moreover, the migration speed of distant and local resident macrophages was decreased upon wounding in the *tlr2* and *myd88* mutants (Fig. 7D and 8D; Fig. 6D and 7D), but not in unchallenged larvae. In summary, our data suggest that TLR signaling regulates neutrophil and macrophage migration upon wounding by controlling their directional persistence and the migration speed of macrophages (Fig. 9).

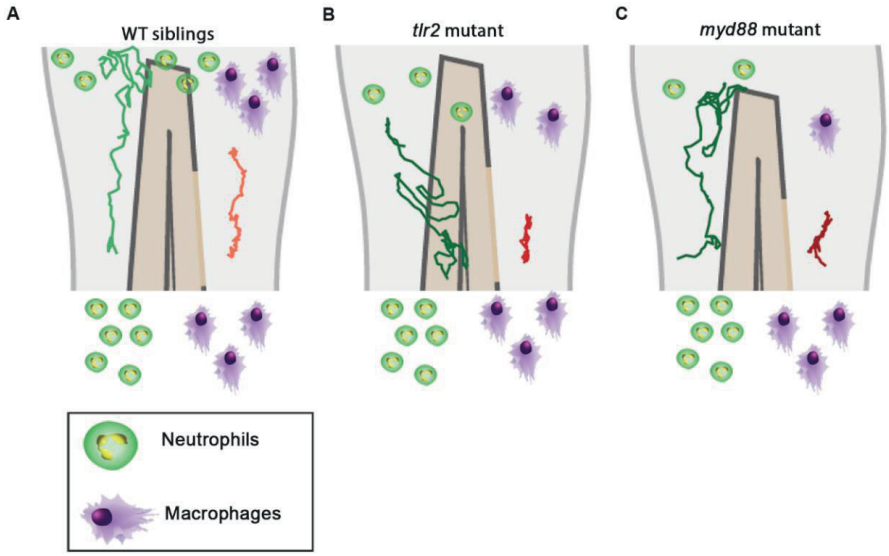

Figure 9 Graphic summary of the data of cell migration behavior in the *tlr2* and *myd88* mutants and wild type siblings.
(A) Cell migration behavior in the wild type siblings.
(B) Cell migration behavior in the *tlr2* mutant.
(C) Cell migration behavior in the *myd88* mutant.
In all cases, the green and red tracks are representative for the medians of the measured total displacements and net displacements in the anteroposterior axis of distant neutrophils and macrophages, respectively. The number of drawn leukocytes at the wound are only representing estimates of the relative numbers in the different genotypes. For the wild type sibling the *tlr2*$^{+/+}$ sibling was used as an example (A).

The difference in directional persistence of the distant neutrophils and macrophages in the mutant shows already within 3 hours post wounding, suggesting that TLR signaling is involved in direct sensing of signals from the wound at the post-transcriptional level. However, since TLRs have not been implied in sensing meandering gradients, we assume that this function involves other receptors. Tlr2 has been shown to be essential for the regulation of cytokines and chemokines expression in both mice and zebrafish [24, 45]. For instance, we have shown that *tlr2* mutant shows a significant lower expression of *cxcl11aa* and also of a related chemokine, *cxcl11ac*, during mycobacterial infection. The CXCR3-CXCL11 chemokine-signaling axis has been demonstrated to play an essential role not only in infection process and but also in inflammation process by regulating leukocyte trafficking [41, 54]. It is possible that an insufficient level of basal transcripts for chemokines at the time of wounding is responsible for the observed defects in leukocyte migration behavior. It is also possible that DAMPs released by dead cells around the wound do not lead to secretion of chemokines in the absence of TLR signaling. DAMPs are well known for activating PRRs and then activating downstream

chemokines and cytokines secretion [13]. Molecules that can function as DAMPs and associated recognition factors during tissue injury such as hyaluronic acid and HMGB1, have been shown to be directly recognized by TLRs in tissues [18, 55, 56]. Chemokines can be produced by leukocytes which are exposed to reactive oxygen species (ROS) produced by injury [2, 57]. Moreover, previous studies have demonstrated that ROS are required for leukocyte recruitment upon wounding in the zebrafish larval model showing its function in long range chemotaxis to arachidonic acid [40, 44]. It has been demonstrated that the generation of ROS is related to TLR signaling in inflammation and tissue injury [58]. For example, Shishido et al. found that TLR2 mediates the generation of ROS after vascular injury [59]. Thus, it is interesting to further study whether the generation of ROS may be altered in *tlr2* and *myd88* mutant zebrafish larvae. In addition, it is possible that the function of other TLRs can be affected in a TLR2 mutant upon tissue wounding. For example, the mRNA expression of TLR4 was decreased in TLR2-deficient mice, which indicated that TLR2 can cooperate with TLR4 to play a role upon tissue wounding [60, 61]. Taken together, these studies suggest that TLR signaling is implicated in the sensitivity to signaling molecules secreted by the wound, explaining why less infiltration of neutrophils and macrophages is observed in tail wounds of the *tlr2* and *myd88* mutants. Future research should be aimed at experiments investigating the cell autonomous nature of the function of TLR signaling in leukocyte cell migration behavior in response to wounding.

To study the mechanistic basis of the differences in cell migratory behavior, mathematical and computational models can also provide insights. Chemokine and ROS gradients can easily be modelled by partial differential equations (PDEs). These can also be incorporated into a cell chemotaxis models, such as random walk models, phase field models, or the Cellular Potts model, with varying degrees of cell resolution, to study the chemotaxis of leukocytes. Such models could provide quantitative insights into how chemokine and ROS gradients affect the migration behavior of the leukocytes, and how the cells change these gradients by binding or secretion of chemokines or absorption and metabolizing ROS (Dona et al., 2013) which is known to affect the robustness of chemotaxis (Tweedy et al., 2016). Using Bayesian inference on tracking data, one can infer a number of chemotaxis parameters, such as the flow rate, diffusion coefficient and production time of the chemoattractant (Manolopoulou et al., 2012). Furthermore, simulated tracks can be compared to experimentally derived tracks. Altogether, such quantitative approaches in close interaction with new experiments could help demonstrate that the chemokine or ROS gradients are affected by the *tlr2* and *myd88* mutations. For such

experiments we will need larger data sets than were currently obtained. This was partially due to the limitations of manual cell tracking. Therefore, in follow-up experiments with larger datasets, the tracking needs to be automated. Consequently, we plan to develop further optimized automatic tracking methods based on the used Viterbi algorithm to quantify larger data sets.

Better theoretical cell migration analysis methods will also be useful for studying subsequent phases of the inflammatory response after wounding [2]. This can assist us in future studies focused on examining the involvement of the TLR signaling in neutrophil reverse migration and in the repair of wounded tissue. Previously we have reported that *myd88* mutant larvae that were raised under germ-free conditions show increased macrophage and decreased neutrophil numbers in the gut [62]. This indicates that the function of TLR signaling in leukocyte migration is dependent on the gut microbiota. It will be highly interesting to test whether the response of leukocytes to tail wounding is also dependent on the microbiome.

Materials and methods

Zebrafish maintenance and strain construction

All animal experiments described in this study were performed at the University of Leiden according to standard protocols (zfin.org) and adhered to the international guidelines specified by the EU Animal Protection Directive 2010/63/EU. The culture of adult fish was approved by the local animal welfare committee (DEC) of the university (License number: protocol 14,198). No adult zebrafish were sacrificed for this study. All experiments were done on 3 days post fertilization (dpf) fish, therefore prior to the free-feeding stage and did not fall under animal experimentation law according to the EU Animal Protection Directive 2010/63/EU. Eggs and larvae were grown at 28.5˚C in egg water (60 g/ml Instant Ocean sea salts). For living imaging and tail wounding experiments, 3 dpf larvae were anesthetized with egg water containing 0.02% buffered 3-aminobenzoic acid ethyl ester (Tricaine, Sigma-Aldrich, the Netherlands).

The *tlr2*^{sa19423} mutant and *myd88*^{hu3568} mutant lines were identified by the sequencing of an ENU-mutagenized zebrafish library [45, 47]. To investigate the effect of the *tlr2* and the *myd88* mutations on leukocyte development, double fluorescent lines *tlr2*$^{+/+}$ *Tg (mpeg1:mCherry-F);TgBAC (mpx: EGFP)*, *tlr2*$^{-/-}$ *Tg (mpeg1:mCherry-F);TgBAC (mpx: EGFP), myd88*$^{+/+}$ *Tg (mpeg1:mCherry-F);TgBAC (mpx: EGFP)*, *myd88*$^{-/-}$ *Tg (mpeg1:mCherry-F);TgBAC (mpx:*

EGFP) were used. Both homozygous mutants were outcrossed with the double transgenic line *Tg (mpeg1:mCherry-F);TgBAC (mpx: EGFP)* [39, 63]. Subsequently, their heterozygous offspring with both positive GFP and mCherry fluorescence were imaged and then used for in-cross. F1 heterozygous in-cross offspring with both positive GFP and mCherry fluorescence were imaged blindly and genotyped post-imaging to produce the homozygous mutants and wild type siblings. In the present study, the double transgenic lines were used for the quantification of cell numbers, cell recruitment assays upon wounding and leukocyte living imaging experiments.

Tail wounding

In the present study, a caudal fin wounding model was applied as previously described [39, 42, 64]. 3 dpf *tlr2* zebrafish larvae were anesthetized with egg water containing 0.02% tricaine (Sigma Aldrich). Subsequently, the caudal fins of larvae were wounded by using a 1 mm sterile sapphire blade scalpel (World Precision Instruments) on a 2% agarose covered petri-dish. To avoid damaging the notochord and other tissues of zebrafish larvae, all of the wounding experiments were performed under a MZ16FA Fluorescence Stereo Microscope (Leica Microsystems, Wetzlar Germany) equipped with a DFC420C color camera (Leica Microsystems). After the wounding, the egg water with 0.02% tricaine was changed with untreated egg water. Wounded larvae were put back into an incubator at 28.5˚C. Subsequently, the wounded larvae were collected or fixed for follow up experiments.

Imaging and quantification

For the quantification of the recruited cell number upon wounding, the double transgenic *tlr2* and *myd88* larvae were wounded with the method described before. 1, 2, 4 and 6 hour post wounding (hpw), larvae were collected and fixed with 4% paraformaldehyde (PFA) in PBS overnight at 4˚C and washed with PBS the next day. The wounded tail area of fixed samples from each group were imaged by using a Leica MZ16FA fluorescence stereo microscope equipped with a DFC420C color camera. Cells localized within an area of 200 µm from the wounding edge toward the body trunk were counted as recruited cells. Analysis was performed by combining three independent experiments.

For detailed cell migration behavior analyses, larvae (3 dpf) were mounted into 1% low melting point agarose (Sigma Aldrich) with 0.02% tricaine and imaged under a Leica TCS SP8 confocal microscope (Leica Microsystems) with a 10× objective (N.A. 0.40). Data were saved as

maximum projection images for further cell counting. The number of neutrophils and macrophages in the tail region were manually quantified.

Live imaging

All time-lapse imaging was performed on 3 dpf larvae. Larvae for each condition (unchallenged/ wounded) were mounted in the method described before and visualized in the CLSM with 1 min time interval for 2 h image capture using a 20× objective (N.A. 0.75). For the manual cell tracking analysis, all time-lapse images were saved as maximum projection images.

We first defined the role of *tlr2* and *myd88* in leukocyte migration under the unchallenged condition. The caudal hematopoietic tissue (CHT) of double transgenic lines was imaged using the CLSM with unchallenged condition. To investigate the effect of the *tlr2* and *myd88* mutations on leukocyte migration upon wounding, the double transgenic line *Tg (mpeg1:mCherry-F);TgBAC (mpx: EGFP)* larvae in the *tlr2*, *myd88* mutant or their wild type background were wounded and performed for real time imaging from 1 hpw to 3 hpw.

Cell tracking and its quantification

The cell tracking of macrophages and neutrophils was either performed manually by using a manual tracking plug-in from Fiji [54, 65] or automatically by using automatic 3D cell tracking algorithms [66, 67]. In this paper, we applied a Viterbi Algorithm, proposed by Magnusson et al. for quantifying leukocyte migration speed [52]. The Viterbi Algorithm follows a global linking strategy which can find the optimal path based on a probabilistically motivated scoring function. The algorithm incorporates six different cell behaviors which include cell migration, migration into or out of image based on probability framework, and cell count, mitosis, apoptosis based on logistic regression. In our application, we did not take into account mitosis and apoptosis. An operation called “swaps” is applied in the Viterbi Algorithm. It can modify links in preexisting tracks if there is a better linking way during a creation of new tracks.

The distance to the wound, mean speed, net displacement, meandering index (M.I.), mean square displacement (MSD), cell diffusivity (D), velocity in anteroposterior direction (V_{AP}) and V_{AP} over time were calculated in different groups by manual tracking data. The calculation and explanation of the parameters are shown in Fig. 4. The distance to the wound is defined as the shortest Euclidean distance to the wound edge (Fig. 4A). For the velocity in the anteroposterior direction, tracks were rotated such that the spines of the larvae were aligned (Fig. 4B). Then,

for each cell the average velocity in the anteroposterior axis was calculated. For V_{AP} over time, the V_{AP} of all cells within a group was averaged over three consecutive time frames. Net displacement, total displacement, meandering index and mean speed are shown in Fig. 4C and Table 1 (Eq. 1-4). The net displacement is the distance of the cell between the first and final time frame (Fig. 4C), i.e., the Euclidian distance traveled being: $d_{net} = d(p_i, p_N)$ (Table 1. Eq. 1). The total displacement is the length of the total cell track, i.e., the sum of the net displacements between two successive frames ($d_{tot} = \sum_{i=1}^{N-1} d(p_i, p_{i+1})$) (Fig. 4C) (Table 1. Eq. 2). Cells can reorient between two frames, such that this measure may underestimate the actual distance traveled. However, we used the same frame rate of 1 min in all experiments, such that the results are comparable with one another. Meandering index is most simply defined as the net distance traveled divided by the total distance traveled (M.I $=\frac{d_{net}}{d_{tot}}$) [68] (Fig. 4C) (Table 1. Eq. 3). Mean speed is the total displacement divided by traveled time ($\bar{v} = \frac{1}{N-1}\sum_{i=1}^{N-1} v_i$) (Table 1. Eq. 4). The MSD at time t was calculated for each group by averaging the squared displacement from starting time t_1=1hpw to time t over all cells (K) within that group ($MSD\ (t) = \frac{1}{K}\sum_{i=1}^{K}\left(d\ (p_{i,1}\ , p_{i,1+t})\right)^2$) (Fig. 4D) (Table 1. Eq. 5). For persistent random walkers, an analytical expression for the MSD exists: $Fitted\ MSD\ (t) = 2v^2\ \tau t - 2(v\tau)^2\ (1 - e^{\frac{-t}{\tau}})$) (Table 1. Eq. 6), with v the intrinsic cell velocity and τ the persistent time, which can be fit to the MSD calculated from cell tracks [69]. The cell diffusivity constant D and MSD (t) at large t are related through $D = 1/2n\ \frac{dMSD(t)}{dt}$, with n=2 the dimension, which for persistent random walkers results in $D = 1/2\ v^2\ \tau$ (Table 1. Eq. 7). We assume that distant neutrophils and macrophages can behave like persistent random walkers during the time span of imaging [70]. We fit Eq. 6 to the MSD curve (Table 1. Eq. 5) using a non-linear least squares method. The obtained parameters v and τ are then used to compute the approximated cell diffusivity D. For distant neutrophils, the fit was performed on the first 80 min of tracking, for distant macrophages, the entire 2h tracking period was used.

The movement behavior of cells can change after they arrive at the wound edge (Fig. S1). To analyze the behavior of leukocyte tracks more accurately, we defined categories of distant and local resident cell movements based on their starting location in the first frame of the time lapse. Cells with a starting point of movements localized further than 200 µm from the wound edge toward to the trunk were categorized as distantly-localized cells (in brief called distant cells).

Cells with a starting point of movements localized within a distance of up to 200 µm from the wound edge toward to the trunk were categorized as wound-residing cells (in brief called local resident cells, Fig. S1A). Although there is no difference between distant neutrophils and local resident neutrophils in mean speed (Fig. S1C), net displacement and meandering index are significantly decreased in the local resident neutrophil groups compared to the distant neutrophil groups (Fig. S1D,E). Furthermore, mean speed, net displacement and meandering index are all significantly decreased in the local resident macrophage groups (Fig. S1F-H). Thus, the cell movement behavior is quantified by separating distant and local resident cell movements in this study.

Table 1. Formulas of calculated track measures and derived measures

Measure	Definition	No.
Net displacement (µm)	$d_{net} = d(p_i, p_N)$	Eq.1
Total displacement (µm)	$d_{tot} = \sum_{i=1}^{N-1} d(p_i, p_{i+1})$	Eq. 2
Meandering index	M.I. = d_{net}/d_{tot}	Eq. 3
Mean speed (µm/min)	$\bar{v} = \frac{1}{N-1}\sum_{i=1}^{N-1} v_i$	Eq. 4
Mean squared displacement (µm^2)	$MSD\ (t) = \frac{1}{K}\sum_{i=1}^{K}(d\ (p_{i,1}\ , p_{i,1+t}))^2$	Eq. 5
Fitted mean squared displacement (µm^2)	$MSD(t) = 2v^2\ \tau t - 2(v\tau)^2\ \left(1 - e^{\frac{-t}{\tau}}\right)$	Eq. 6
Cell diffusivity constant D (µm^2/min)	$D = 1/2\ v^2\ \tau$	Eq. 7

Statistical analysis

Graphpad Prism software (Version 8.1.1; GraphPad Software, San Diego, CA, USA) was used for statistical analysis. Computations of distance to the wound, MSD and V_{AP} were performed using a Python script including the SciPy stats library for statistical testing. Shaded regions of MSD and V_{AP} over time indicate standard error of mean, the other experiment data are shown as mean ± SD. Statistical significance of differences was determined by using an unpaired, two-tailed t-test for comparing the difference between wild type and *tlr2* and *myd88* mutant. (ns, no significant difference; *P < 0.05; **P < 0.01; ***P < 0.001; ****P < 0.0001).

Acknowledgments

We acknowledge Ulrike Nehrdich and Guus van der Velden for the assistance in adult zebrafish care.

Reference

1. Lieschke GJ, Oates AC, Crowhurst MO, Ward AC, Layton JE. Morphologic and functional characterization of granulocytes and macrophages in embryonic and adult zebrafish. Blood. 2001;98(10):3087-96. Epub 2001/11/08. doi: 10.1182/blood.v98.10.3087. PubMed PMID: 11698295.

2. Soehnlein O, Lindbom L. Phagocyte partnership during the onset and resolution of inflammation. Nat Rev Immunol. 2010;10(6):427-39. Epub 2010/05/26. doi: 10.1038/nri2779. PubMed PMID: 20498669.

3. Serhan CN, Brain SD, Buckley CD, Gilroy DW, Haslett C, O'Neill LA, et al. Resolution of inflammation: state of the art, definitions and terms. FASEB J. 2007;21(2):325-32. Epub 2007/02/03. doi: 10.1096/fj.06-7227rev. PubMed PMID: 17267386; PubMed Central PMCID: PMCPMC3119634.

4. Li L, Yan B, Shi YQ, Zhang WQ, Wen ZL. Live imaging reveals differing roles of macrophages and neutrophils during zebrafish tail fin regeneration. J Biol Chem. 2012;287(30):25353-60. Epub 2012/05/11. doi: 10.1074/jbc.M112.349126. PubMed PMID: 22573321; PubMed Central PMCID: PMCPMC3408142.

5. Nathan C. Neutrophils and immunity: challenges and opportunities. Nat Rev Immunol. 2006;6(3):173-82. Epub 2006/02/25. doi: 10.1038/nri1785. PubMed PMID: 16498448.

6. Weiss SJ. Tissue destruction by neutrophils. N Engl J Med. 1989;320(6):365-76. Epub 1989/02/09. doi: 10.1056/NEJM198902093200606. PubMed PMID: 2536474.

7. Brazil JC, Louis NA, Parkos CA. The role of polymorphonuclear leukocyte trafficking in the perpetuation of inflammation during inflammatory bowel disease. Inflamm Bowel Dis. 2013;19(7):1556-65. Epub 2013/04/20. doi: 10.1097/MIB.0b013e318281f54e. PubMed PMID: 23598816; PubMed Central PMCID: PMCPMC4110963.

8. Mescher AL. Macrophages and fibroblasts during inflammation and tissue repair in models of organ regeneration. Regeneration (Oxf). 2017;4(2):39-53. Epub 2017/06/16. doi: 10.1002/reg2.77. PubMed PMID: 28616244; PubMed Central PMCID: PMCPMC5469729.

9. Martin P, Leibovich SJ. Inflammatory cells during wound repair: the good, the bad and the ugly. Trends Cell Biol. 2005;15(11):599-607. Epub 2005/10/06. doi: 10.1016/j.tcb.2005.09.002. PubMed PMID: 16202600.

10. Hopkin SJ, Lewis JW, Krautter F, Chimen M, McGettrick HM. Triggering the Resolution of Immune Mediated Inflammatory Diseases: Can Targeting Leukocyte Migration Be the Answer? Front Pharmacol. 2019;10:184. Epub 2019/03/19. doi: 10.3389/fphar.2019.00184. PubMed PMID: 30881306; PubMed Central PMCID: PMCPMC6407428.

11. Hato T, Dagher PC. How the Innate Immune System Senses Trouble and Causes Trouble. Clin J Am Soc Nephrol. 2015;10(8):1459-69. Epub 2014/11/22. doi: 10.2215/CJN.04680514. PubMed PMID: 25414319; PubMed Central PMCID: PMCPMC4527020.

12. Janeway CA, Jr., Medzhitov R. Innate immune recognition. Annu Rev Immunol. 2002;20:197-216. Epub 2002/02/28. doi: 10.1146/annurev.immunol.20.083001.084359. PubMed PMID: 11861602.

13. Niethammer P. The early wound signals. Curr Opin Genet Dev. 2016;40:17-22. Epub 2016/06/09. doi: 10.1016/j.gde.2016.05.001. PubMed PMID: 27266971; PubMed Central PMCID: PMCPMC5278878.

14. Vijay K. Toll-like receptors in immunity and inflammatory diseases: Past, present, and future. Int Immunopharmacol. 2018;59:391-412. Epub 2018/05/08. doi: 10.1016/j.intimp.2018.03.002. PubMed PMID: 29730580; PubMed Central PMCID: PMCPMC7106078.

15. Yu L, Wang L, Chen S. Endogenous toll-like receptor ligands and their biological significance. J Cell Mol Med. 2010;14(11):2592-603. Epub 2010/07/16. doi: 10.1111/j.1582-4934.2010.01127.x. PubMed PMID: 20629986; PubMed Central PMCID: PMCPMC4373479.

16. Quesniaux VJ, Nicolle DM, Torres D, Kremer L, Guerardel Y, Nigou J, et al. Toll-like receptor 2 (TLR2)-dependent-positive and TLR2-independent-negative regulation of proinflammatory cytokines by mycobacterial lipomannans. J Immunol. 2004;172(7):4425-34. Epub 2004/03/23. doi: 10.4049/jimmunol.172.7.4425. PubMed PMID: 15034058.

17. Poltorak A, He X, Smirnova I, Liu MY, Van Huffel C, Du X, et al. Defective LPS signaling in C3H/HeJ and C57BL/10ScCr mice: mutations in Tlr4 gene. Science. 1998;282(5396):2085-8. Epub 1998/12/16. doi: 10.1126/science.282.5396.2085. PubMed PMID: 9851930.

18. Bianchi ME. HMGB1 loves company. J Leukoc Biol. 2009;86(3):573-6. Epub 2009/05/06. doi: 10.1189/jlb.1008585. PubMed PMID: 19414536.

19. Yanai H, Ban T, Wang Z, Choi MK, Kawamura T, Negishi H, et al. HMGB proteins function as universal sentinels for nucleic-acid-mediated innate immune responses. Nature. 2009;462(7269):99-103. Epub 2009/11/06. doi: 10.1038/nature08512. PubMed PMID: 19890330.

20. Teixeira HS, Zhao J, Kazmierski E, Kinane DF, Benakanakere MR. TLR3-Dependent Activation of TLR2 Endogenous Ligands via the MyD88 Signaling Pathway Augments the Innate Immune Response. Cells. 2020;9(8). Epub 2020/08/23. doi: 10.3390/cells9081910. PubMed PMID: 32824595; PubMed Central PMCID: PMCPMC7464415.

21. Oliveira-Nascimento L, Massari P, Wetzler LM. The Role of TLR2 in Infection and Immunity. Front Immunol. 2012;3:79. Epub 2012/05/09. doi: 10.3389/fimmu.2012.00079. PubMed PMID: 22566960; PubMed Central PMCID: PMCPMC3342043.

22. Schauber J, Dorschner RA, Coda AB, Buchau AS, Liu PT, Kiken D, et al. Injury enhances TLR2 function and antimicrobial peptide expression through a vitamin D-dependent mechanism. J Clin Invest. 2007;117(3):803-11. Epub 2007/02/10. doi: 10.1172/JCI30142. PubMed PMID: 17290304; PubMed Central PMCID: PMCPMC1784003.

23. Xu Y, Zhou Y, Lin H, Hu H, Wang Y, Xu G. Toll-like receptor 2 in promoting angiogenesis after acute ischemic injury. Int J Mol Med. 2013;31(3):555-60. Epub 2013/01/15. doi: 10.3892/ijmm.2013.1240. PubMed PMID: 23314218.

24. Moles A, Murphy L, Wilson CL, Chakraborty JB, Fox C, Park EJ, et al. A TLR2/S100A9/CXCL-2 signaling network is necessary for neutrophil recruitment in acute and chronic liver injury in the mouse. J Hepatol. 2014;60(4):782-91. Epub 2013/12/18. doi: 10.1016/j.jhep.2013.12.005. PubMed PMID: 24333183; PubMed Central PMCID: PMCPMC3960359.

25. Castoldi A, Braga TT, Correa-Costa M, Aguiar CF, Bassi EJ, Correa-Silva R, et al. TLR2, TLR4 and the MYD88 signaling pathway are crucial for neutrophil migration in acute kidney injury induced by sepsis. PLoS One. 2012;7(5):e37584. Epub 2012/06/02. doi: 10.1371/journal.pone.0037584. PubMed PMID: 22655058; PubMed Central PMCID: PMCPMC3360043.

26. Mojumdar K, Giordano C, Lemaire C, Liang F, Divangahi M, Qureshi ST, et al. Divergent impact of Toll-like receptor 2 deficiency on repair mechanisms in healthy muscle versus Duchenne muscular dystrophy. J Pathol. 2016;239(1):10-22. Epub 2016/01/23. doi: 10.1002/path.4689. PubMed PMID: 26800321.

27. Kim D, You B, Lim H, Lee SJ. Toll-like receptor 2 contributes to chemokine gene expression and macrophage infiltration in the dorsal root ganglia after peripheral nerve injury. Mol Pain. 2011;7:74. Epub 2011/09/29. doi: 10.1186/1744-8069-7-74. PubMed PMID: 21951975; PubMed Central PMCID: PMCPMC3192680.

28. Seki E, Park E, Fujimoto J. Toll-like receptor signaling in liver regeneration, fibrosis and carcinogenesis. Hepatol Res. 2011;41(7):597-610. Epub 2011/06/24. doi: 10.1111/j.1872-034X.2011.00822.x. PubMed PMID: 21696522; PubMed Central PMCID: PMCPMC3754784.

29. Miura K, Yang L, van Rooijen N, Brenner DA, Ohnishi H, Seki E. Toll-like receptor 2 and palmitic acid cooperatively contribute to the development of nonalcoholic steatohepatitis through inflammasome activation in mice. Hepatology. 2013;57(2):577-89. Epub 2012/09/19. doi: 10.1002/hep.26081. PubMed PMID: 22987396; PubMed Central PMCID: PMCPMC3566276.

30. Ji L, Xue R, Tang W, Wu W, Hu T, Liu X, et al. Toll like receptor 2 knock-out attenuates carbon tetrachloride (CCl4)-induced liver fibrosis by downregulating MAPK and NF-kappaB signaling pathways. FEBS Lett. 2014;588(12):2095-100. Epub 2014/05/13. doi: 10.1016/j.febslet.2014.04.042. PubMed PMID: 24815695.

31. Deng Q, Harvie EA, Huttenlocher A. Distinct signalling mechanisms mediate neutrophil attraction to bacterial infection and tissue injury. Cell Microbiol. 2012;14(4):517-28. Epub 2011/12/23. doi: 10.1111/j.1462-5822.2011.01738.x. PubMed PMID: 22188170; PubMed Central PMCID: PMCPMC3302966.

32. Chen L, Zheng L, Chen P, Liang G. Myeloid Differentiation Primary Response Protein 88 (MyD88): The Central Hub of TLR/IL-1R Signaling. J Med Chem. 2020. Epub 2020/09/16. doi: 10.1021/acs.jmedchem.0c00884. PubMed PMID: 32931267.

33. Takeda K, Akira S. Microbial recognition by Toll-like receptors. J Dermatol Sci. 2004;34(2):73-82. Epub 2004/03/23. doi: 10.1016/j.jdermsci.2003.10.002. PubMed PMID: 15033189.

34. Wagner N, Reinehr S, Palmhof M, Schuschel D, Tsai T, Sommer E, et al. Microglia Activation in Retinal Ischemia Triggers Cytokine and Toll-Like Receptor Response. J Mol Neurosci. 2020. Epub 2020/08/25. doi: 10.1007/s12031-020-01674-w. PubMed PMID: 32833183.

35. Dasu MR, Thangappan RK, Bourgette A, DiPietro LA, Isseroff R, Jialal I. TLR2 expression and signaling-dependent inflammation impair wound healing in diabetic mice. Lab Invest. 2010;90(11):1628-36. Epub 2010/08/25. doi: 10.1038/labinvest.2010.158. PubMed PMID: 20733560.

36. Macedo L, Pinhal-Enfield G, Alshits V, Elson G, Cronstein BN, Leibovich SJ. Wound healing is impaired in MyD88-deficient mice: a role for MyD88 in the regulation of wound healing by adenosine A2A receptors. Am J Pathol. 2007;171(6):1774-88. Epub 2007/11/03. doi: 10.2353/ajpath.2007.061048. PubMed PMID: 17974599; PubMed Central PMCID: PMCPMC2111102.

37. Houseright RA, Rosowski EE, Lam PY, Tauzin SJM, Mulvaney O, Dewey CN, et al. Cell type specific gene expression profiling reveals a role for complement component C3 in neutrophil responses to tissue damage. Sci Rep. 2020;10(1):15716. Epub 2020/09/26. doi: 10.1038/s41598-020-72750-9. PubMed PMID: 32973200; PubMed Central PMCID: PMCPMC7518243.

38. Meijer AH, Spaink HP. Host-pathogen interactions made transparent with the zebrafish model. Curr Drug Targets. 2011;12(7):1000-17. Epub 2011/03/04. doi: 10.2174/138945011795677809. PubMed PMID: 21366518; PubMed Central PMCID: PMCPMC3319919.

39. Renshaw SA, Loynes CA, Trushell DM, Elworthy S, Ingham PW, Whyte MK. A transgenic zebrafish model of neutrophilic inflammation. Blood. 2006;108(13):3976-8. Epub 2006/08/24. doi: 10.1182/blood-2006-05-024075. PubMed PMID: 16926288.

40. Niethammer P, Grabher C, Look AT, Mitchison TJ. A tissue-scale gradient of hydrogen peroxide mediates rapid wound detection in zebrafish. Nature. 2009;459(7249):996-9. Epub 2009/06/06. doi: 10.1038/nature08119. PubMed PMID: 19494811; PubMed Central PMCID: PMCPMC2803098.

41. Sommer F, Torraca V, Kamel SM, Lombardi A, Meijer AH. Frontline Science: Antagonism between regular and atypical Cxcr3 receptors regulates macrophage migration during infection and injury in zebrafish. J Leukoc Biol. 2020;107(2):185-203. Epub 2019/09/19. doi: 10.1002/JLB.2HI0119-006R. PubMed PMID: 31529512; PubMed Central PMCID: PMCPMC7028096.

42. Xie Y, Tolmeijer S, Oskam JM, Tonkens T, Meijer AH, Schaaf MJM. Glucocorticoids inhibit macrophage differentiation towards a pro-inflammatory phenotype upon wounding without affecting their migration. Dis Model Mech. 2019;12(5). Epub 2019/05/11. doi: 10.1242/dmm.037887. PubMed PMID: 31072958; PubMed Central PMCID: PMCPMC6550045.

43. Bernut A, Loynes CA, Floto RA, Renshaw SA. Deletion of cftr Leads to an Excessive Neutrophilic Response and Defective Tissue Repair in a Zebrafish Model of Sterile Inflammation. Front Immunol. 2020;11:1733. Epub 2020/08/28. doi: 10.3389/fimmu.2020.01733. PubMed PMID: 32849617; PubMed Central PMCID: PMCPMC7412881.

44. Katikaneni A, Jelcic M, Gerlach GF, Ma Y, Overholtzer M, Niethammer P. Lipid peroxidation regulates long-range wound detection through 5-lipoxygenase in zebrafish. Nat Cell Biol. 2020;22(9):1049-55. Epub 2020/09/02. doi: 10.1038/s41556-020-0564-2. PubMed PMID: 32868902.

45. Hu W, Yang S, Shimada Y, Munch M, Marin-Juez R, Meijer AH, et al. Infection and RNA-seq analysis of a zebrafish tlr2 mutant shows a broad function of this toll-like receptor in transcriptional and metabolic control and defense to Mycobacterium marinum infection. BMC Genomics. 2019;20(1):878. Epub 2019/11/22. doi: 10.1186/s12864-019-6265-1. PubMed PMID: 31747871; PubMed Central PMCID: PMCPMC6869251.

46. Henry KM, Loynes CA, Whyte MK, Renshaw SA. Zebrafish as a model for the study of neutrophil biology. J Leukoc Biol. 2013;94(4):633-42. Epub 2013/03/07. doi: 10.1189/jlb.1112594. PubMed PMID: 23463724.

47. van der Vaart M, van Soest JJ, Spaink HP, Meijer AH. Functional analysis of a zebrafish myd88 mutant identifies key transcriptional components of the innate immune system. Dis Model Mech. 2013;6(3):841-54. Epub 2013/03/09. doi: 10.1242/dmm.010843. PubMed PMID: 23471913; PubMed Central PMCID: PMCPMC3634667.

48. Meijer AH, Gabby Krens SF, Medina Rodriguez IA, He S, Bitter W, Ewa Snaar-Jagalska B, et al. Expression analysis of the Toll-like receptor and TIR domain adaptor families of zebrafish. Mol Immunol. 2004;40(11):773-83. Epub 2003/12/23. doi: 10.1016/j.molimm.2003.10.003. PubMed PMID: 14687934.

49. Yang S, Marin-Juez R, Meijer AH, Spaink HP. Common and specific downstream signaling targets controlled by Tlr2 and Tlr5 innate immune signaling in zebrafish. BMC Genomics. 2015;16:547. Epub 2015/07/26. doi: 10.1186/s12864-015-1740-9. PubMed PMID: 26208853; PubMed Central PMCID: PMCPMC4514945.

50. He M, Halima M, Xie YF, Schaaf MJM, Meijer AH, Wang M. Ginsenoside Rg1 Acts as a Selective Glucocorticoid Receptor Agonist with Anti-Inflammatory Action without Affecting Tissue Regeneration in Zebrafish Larvae. Cells. 2020;9(5). doi: 10.3390/cells9051107. PubMed PMID: WOS:000539340200041.

51. Sommer F, Ortiz Zacari As NV, Heitman LH, Meijer AH. Inhibition of macrophage migration in zebrafish larvae demonstrates in vivo efficacy of human CCR2 inhibitors. Dev Comp Immunol. 2020;116:103932. Epub 2020/11/26. doi: 10.1016/j.dci.2020.103932. PubMed PMID: 33238180.

52. Magnusson KEG, Jalden J, Gilbert PM, Blau HM. Global Linking of Cell Tracks Using the Viterbi Algorithm. Ieee Transactions on Medical Imaging. 2015;34(4):911-29. doi: 10.1109/Tmi.2014.2370951. PubMed PMID: WOS:000352533200008.

53. Gray C, Loynes CA, Whyte MK, Crossman DC, Renshaw SA, Chico TJ. Simultaneous intravital imaging of macrophage and neutrophil behaviour during inflammation using a novel transgenic zebrafish. Thromb Haemost. 2011;105(5):811-9. Epub 2011/01/13. doi: 10.1160/TH10-08-0525. PubMed PMID: 21225092.

54. Torraca V, Cui C, Boland R, Bebelman JP, van der Sar AM, Smit MJ, et al. The CXCR3-CXCL11 signaling axis mediates macrophage recruitment and dissemination of mycobacterial infection. Dis Model Mech. 2015;8(3):253-69. Epub 2015/01/13. doi: 10.1242/dmm.017756. PubMed PMID: 25573892; PubMed Central PMCID: PMCPMC4348563.

55. Jiang D, Liang J, Fan J, Yu S, Chen S, Luo Y, et al. Regulation of lung injury and repair by Toll-like receptors and hyaluronan. Nat Med. 2005;11(11):1173-9. Epub 2005/10/26. doi: 10.1038/nm1315. PubMed PMID: 16244651.

56. Komai K, Shichita T, Ito M, Kanamori M, Chikuma S, Yoshimura A. Role of scavenger receptors as damage-associated molecular pattern receptors in Toll-like receptor activation. Int Immunol. 2017;29(2):59-70. Epub 2017/03/25. doi: 10.1093/intimm/dxx010. PubMed PMID: 28338748.

57. Yamamoto S, Shimizu S, Kiyonaka S, Takahashi N, Wajima T, Hara Y, et al. TRPM2-mediated Ca2+influx induces chemokine production in monocytes that aggravates inflammatory neutrophil infiltration. Nat Med. 2008;14(7):738-47. Epub 2008/06/11. doi: 10.1038/nm1758. PubMed PMID: 18542050; PubMed Central PMCID: PMCPMC2789807.

58. Mittal M, Siddiqui MR, Tran K, Reddy SP, Malik AB. Reactive oxygen species in inflammation and tissue injury. Antioxid Redox Signal. 2014;20(7):1126-67. Epub 2013/09/03. doi: 10.1089/ars.2012.5149. PubMed PMID: 23991888; PubMed Central PMCID: PMCPMC3929010.

59. Shishido T, Nozaki N, Takahashi H, Arimoto T, Niizeki T, Koyama Y, et al. Central role of endogenous Toll-like receptor-2 activation in regulating inflammation, reactive oxygen species production, and subsequent neointimal formation after vascular injury. Biochem Biophys Res Commun. 2006;345(4):1446-53. Epub 2006/05/30. doi: 10.1016/j.bbrc.2006.05.056. PubMed PMID: 16730663.

60. Suga H, Sugaya M, Fujita H, Asano Y, Tada Y, Kadono T, et al. TLR4, rather than TLR2, regulates wound healing through TGF-beta and CCL5 expression. J Dermatol Sci. 2014;73(2):117-24. Epub 2013/11/21. doi: 10.1016/j.jdermsci.2013.10.009. PubMed PMID: 24252748.

61. Chen L, DiPietro LA. Toll-Like Receptor Function in Acute Wounds. Advances in Wound Care. 2017;6(10):344-55. doi: 10.1089/wound.2017.0734. PubMed PMID: WOS:000412015700004.

62. Koch BEV, Yang S, Lamers G, Stougaard J, Spaink HP. Author Correction: Intestinal microbiome adjusts the innate immune setpoint during colonization through negative regulation of MyD88. Nat Commun. 2019;10(1):526. Epub 2019/01/30. doi: 10.1038/s41467-019-08456-y. PubMed PMID: 30692545; PubMed Central PMCID: PMCPMC6349902.

63. Bernut A, Herrmann JL, Kissa K, Dubremetz JF, Gaillard JL, Lutfalla G, et al. Mycobacterium abscessus cording prevents phagocytosis and promotes abscess formation. Proc Natl Acad Sci U S A. 2014;111(10):E943-52. Epub 2014/02/26. doi: 10.1073/pnas.1321390111. PubMed PMID: 24567393; PubMed Central PMCID: PMCPMC3956181.

64. Chatzopoulou A, Heijmans JP, Burgerhout E, Oskam N, Spaink HP, Meijer AH, et al. Glucocorticoid-Induced Attenuation of the Inflammatory Response in Zebrafish. Endocrinology. 2016;157(7):2772-84. Epub 2016/05/25. doi: 10.1210/en.2015-2050. PubMed PMID: 27219276.

65. Meijering E, Dzyubachyk O, Smal I. Methods for cell and particle tracking. Methods Enzymol. 2012;504:183-200. Epub 2012/01/24. doi: 10.1016/B978-0-12-391857-4.00009-4. PubMed PMID: 22264535.

66. Tinevez JY, Perry N, Schindelin J, Hoopes GM, Reynolds GD, Laplantine E, et al. TrackMate: An open and extensible platform for single-particle tracking. Methods. 2017;115:80-90. Epub 2016/10/08. doi: 10.1016/j.ymeth.2016.09.016. PubMed PMID: 27713081.

67. Ulman V, Maska M, Magnusson KEG, Ronneberger O, Haubold C, Harder N, et al. An objective comparison of cell-tracking algorithms. Nat Methods. 2017;14(12):1141-52. Epub 2017/10/31. doi: 10.1038/nmeth.4473. PubMed PMID: 29083403; PubMed Central PMCID: PMCPMC5777536.

68. Stokes CL, Lauffenburger DA, Williams SK. Migration of individual microvessel endothelial cells: stochastic model and parameter measurement. J Cell Sci. 1991;99 (Pt 2):419-30. Epub 1991/06/01. PubMed PMID: 1885678.

69. Selmeczi D, Mosler S, Hagedorn PH, Larsen NB, Flyvbjerg H. Cell motility as persistent random motion: Theories from experiments. Biophysical Journal. 2005;89(2):912-31. doi: 10.1529/biophysj.105.061150. PubMed PMID: WOS:000230822200017.

70. Taylor HB, Liepe J, Barthen C, Bugeon L, Huvet M, Kirk PDW, et al. P38 and JNK have opposing effects on persistence of in vivo leukocyte migration in zebrafish. Immunology and Cell Biology. 2013;91(1):60-9. doi: 10.1038/icb.2012.57. PubMed PMID: WOS:000313549700010.

Supplementary Material

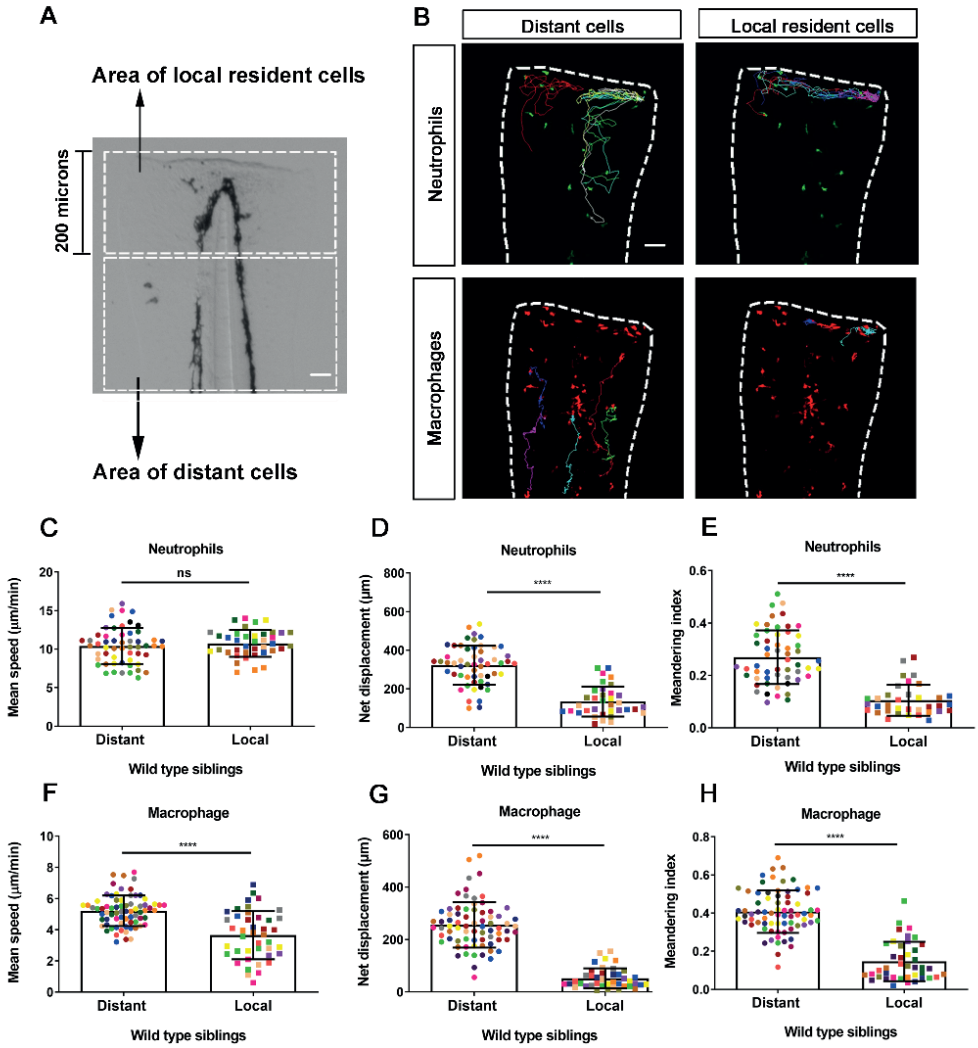

Supplementary Figure 1 (A) Schematic diagram of distant and local resident cell migration. (B) Representative images of the distant cell tracks and local resident cell tracks. (C-D) Quantification of the distant neutrophil tracks and the local resident neutrophil tracks. Statistical analyses were done with 15 and 13 fish, respectively, for each group. Sample size (n): 55, 39. (F-H) Quantification of the distant macrophage tracks and the local resident tracks. Statistical analyses were done with 15 fish for each group. Sample size (n): 73, 41. In all cases, each color indicates a different larva. An unpaired, two-tailed t-test was used to assess significance (ns, non-significance) and data are shown as mean± SD. Scale bar: 50 μm.

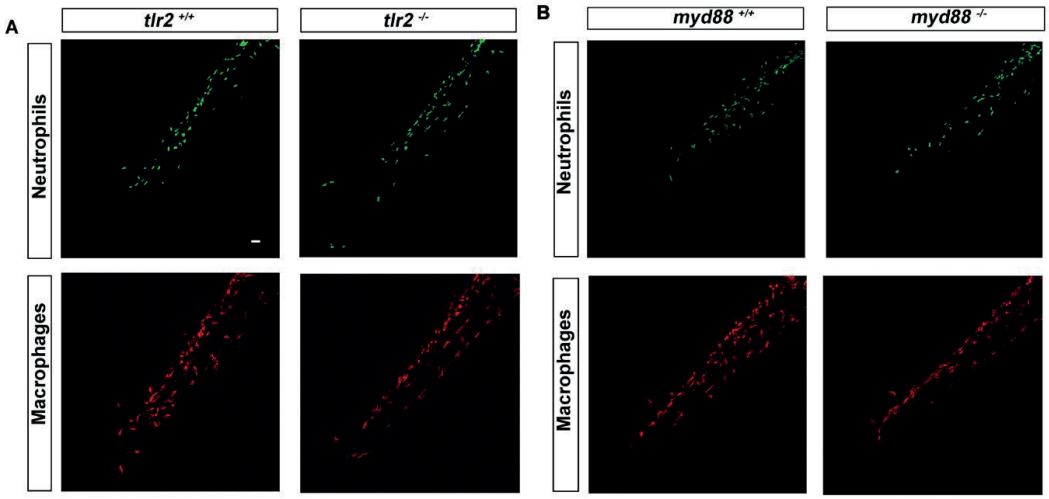

Supplementary Figure 2 Representative images of the quantification of cell numbers in tail region. The pictures of *tlr2*$^{+/+}$, *tlr2*$^{-/-}$ (A), *myd88*$^{+/+}$ and *myd88*$^{-/-}$ (B) zebrafish larvae were taken at 3 dpf for quantifying the number of neutrophils and macrophages.

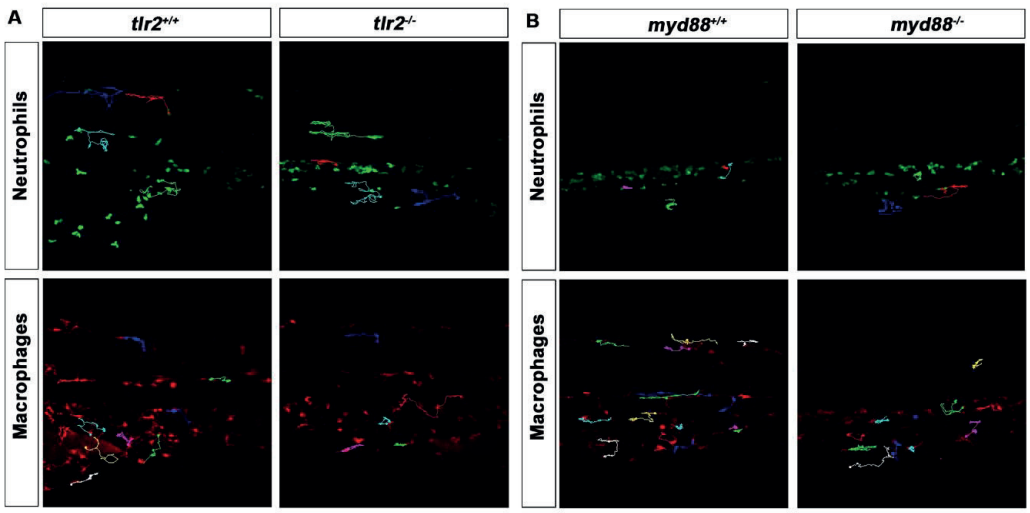

Supplementary Figure 3 Representative images of the neutrophil and macrophage basal migratory tracks in *tlr2* and *myd88* zebrafish. The cell tracks of 3 dpf *tlr2*$^{+/+}$, *tlr2*$^{-/-}$ (A), *myd88*$^{+/+}$ and *myd88*$^{-/-}$ (B) zebrafish larvae were tracked for 2 h and images were taken every 1 min by using a confocal microscope for quantifying cells basal migratory capability.

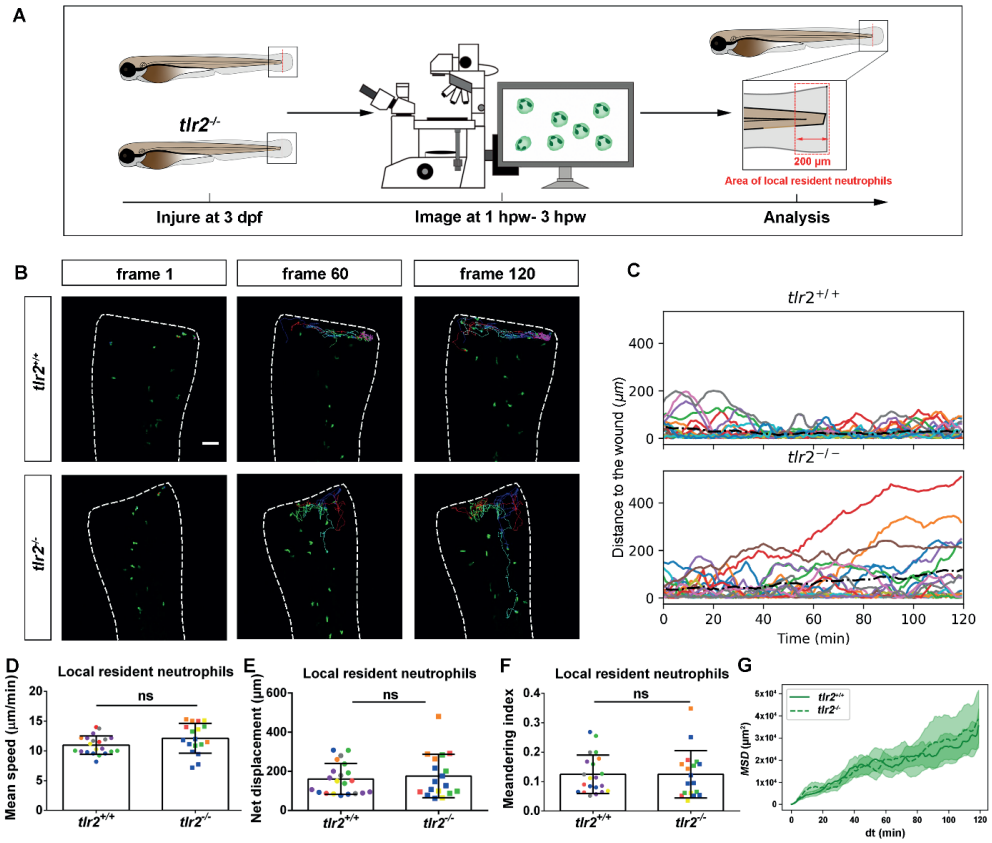

Supplementary Figure 4 Quantification of localized resident neutrophils behavior in wounded *tlr2* larvae. (A) Experimental scheme. (B) Representative images of local resident neutrophils tracks in the wounded tail fin of 3 dpf *tlr2*$^{+/+}$ or *tlr2*$^{-/-}$ larvae at frame 1, frame 60 and frame 120. Cell tracking movies are shown in Supplementary Movie S17-18). Scale bar: 50 µm. (C) Distance to the wound. Black dash line represents average distance to the wound. Each color line represents one cell. (D-I) Quantification of local resident neutrophil tracks, mean speed (D); net displacement (E); Meandering index (F); MSD (G). In panel D-F and H, each color indicates a different larva. Statistical analyses were done with 7 and 5 fish, respectively, for each group. An unpaired, two-tailed t-test was used to assess significance (ns, non-significance) and data are shown as mean± SD. Sample size (n): 21, 18.

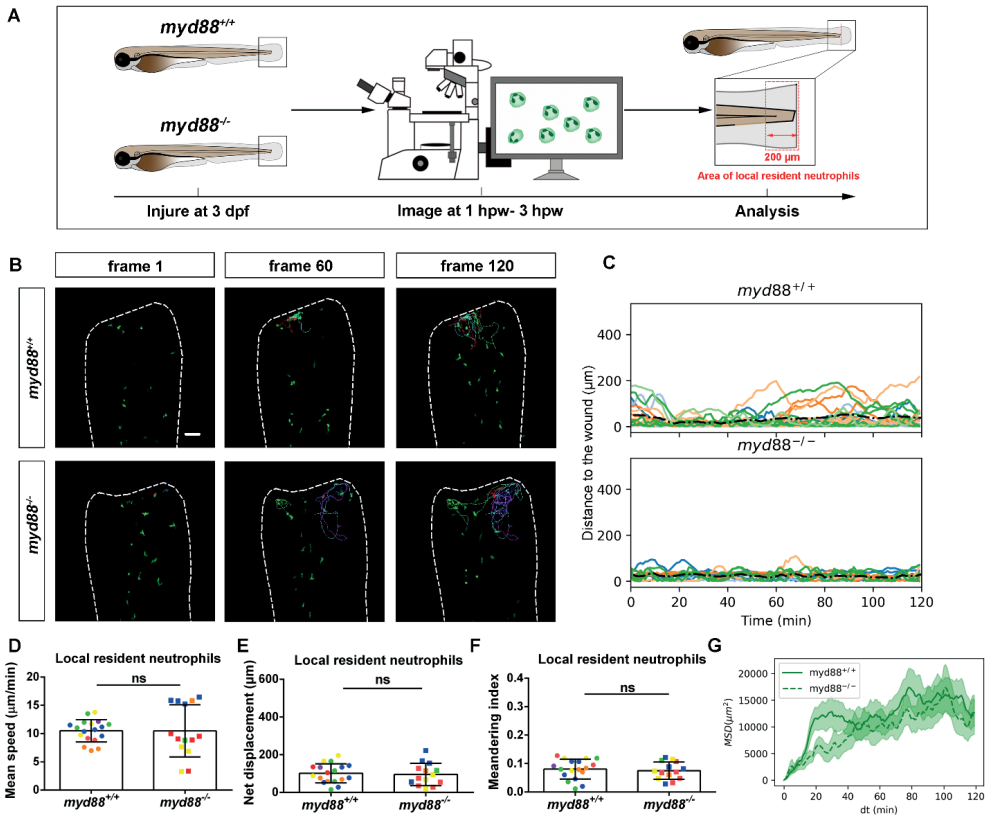

Supplementary Figure 5 Quantification of localized resident neutrophils behavior in wounded *myd88* larvae. (A) Experimental scheme. (B) Representative images of local resident neutrophils tracks in the wounded tail fin of 3 dpf *myd88*$^{+/+}$ or *myd88*$^{-/-}$ larvae at frame 1, frame 60 and frame 120. Cell tracking movies are shown in Supplementary Movie S19-20). Scale bar: 50 µm. (C) Distance to the wound. Black dash line represents average distance to the wound. Each color line represents one cell. (D-I) Quantification of local resident neutrophil tracks, mean speed (D); net displacement (E); Meandering index (F); MSD (G). In panel D-F and H, each color indicates a different larva. Statistical analyses were done with 6 and 5 fish, respectively, for each group. An unpaired, two-tailed t-test was used to assess significance (ns, non-significance) and data are shown as mean± SD. Sample size (n): 18, 14

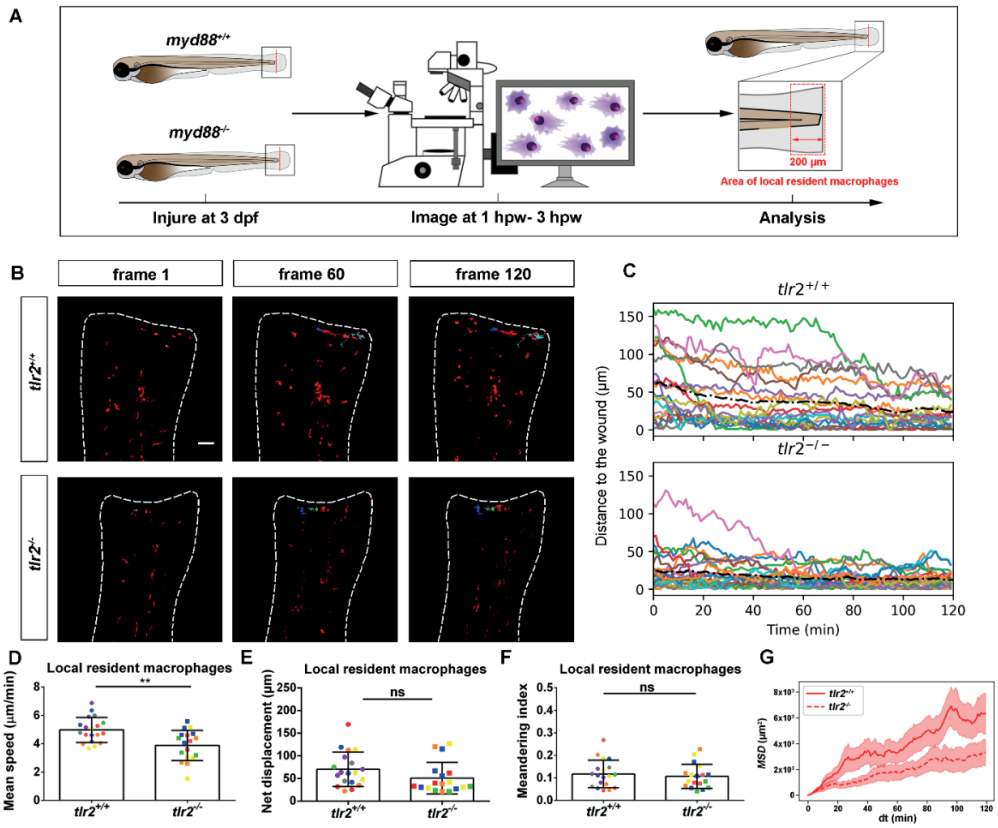

Supplementary Figure 6 Quantification of localized resident macrophages behavior in wounded *tlr2* larvae. (A) Experimental scheme. (B) Representative images of local resident macrophages tracks in the wounded tail fin of 3 dpf $tlr2^{+/+}$ or $tlr2^{-/-}$ larvae at frame 1, frame 60 and frame 120. Cell tracking movies are shown in Supplementary Movie S21-22). Scale bar: 50 µm. (C) Distance to the wound. Black dash line represents average distance to the wound. Each color line represents one cell. (D-I) Quantification of local resident macrophage tracks, mean speed (D); net displacement (E); Meandering index (F); MSD (G). In panel D-F and H, each color indicates a different larva. Statistical analyses were done with 7 and 5 fish, respectively, for each group. An unpaired, two-tailed t-test was used to assess significance (ns, non-significance) and data are shown as mean± SD. Sample size (n): 19, 18.

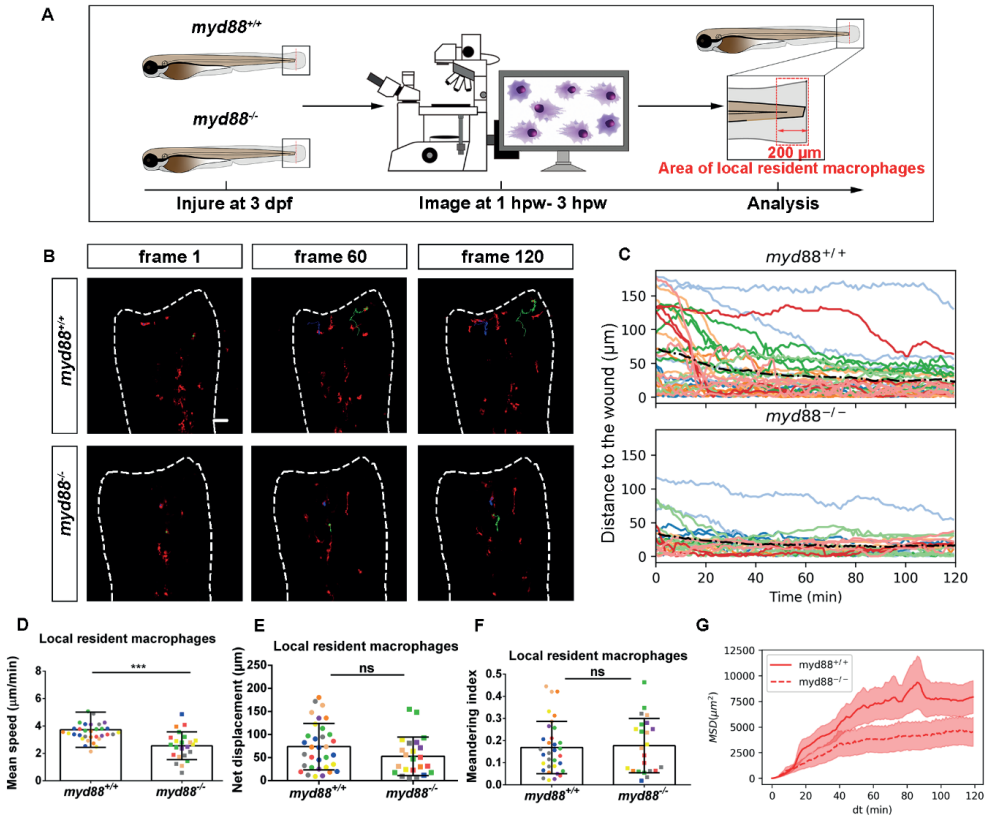

Supplementary Figure 7 Quantification of localized resident macrophages behavior in wounded *myd88* larvae. (A) Experimental scheme. (B) Representative images of local resident macrophages tracks in the wounded tail fin of 3 dpf *myd88*$^{+/+}$ or *myd88*$^{-/-}$ larvae at frame 1, frame 60 and frame 120. Scale bar: 50 µm. (C) Distance to the wound. Black dash line represents average distance to the wound. Each color line represents one cell. Cell tracking movies are shown in Supplementary Movie S23-24). (D-I) Quantification of local resident macrophage tracks, mean speed (D); net displacement (E); Meandering index (F); MSD (G). In panel D-F and H, each color indicates a different larva. Statistical analyses were done with 8 and 8 fish, respectively, for each group. An unpaired, two-tailed t-test was used to assess significance (ns, non-significance) and data are shown as mean± SD. Sample size (n): 33, 23.

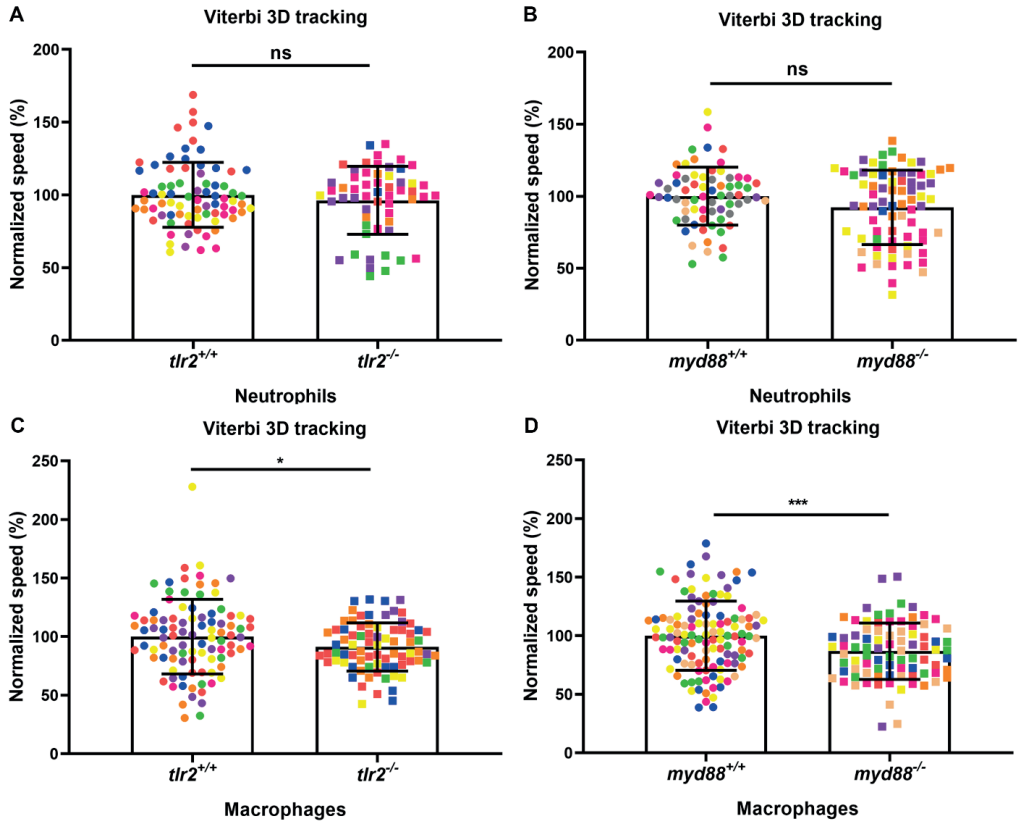

Supplementary Figure 8 Quantification of tracks using automatic Viterbi Algorithm. (A) Quantification of neutrophil behavior in wounded *tlr2* larvae. Statistical analyses were done with 7 fish, for each group. Sample size (n): 77, 56. (B) Quantification of neutrophil behavior in wounded *myd88* larvae. Statistical analyses were done with 9 or 8 fish, respectively, for each group. Sample size (n): 69, 76. (C) Quantification of macrophage behavior in wounded *tlr2* larvae. Statistical analyses were done with 7 fish, for each group. Sample size (n): 95, 78. (D) Quantification of macrophage behavior in wounded *myd88* larvae. Statistical analyses were done with 8 fish, for each group. Sample size (n): 119, 85.In all cases, an unpaired, two-tailed t-test was used to assess significance (ns, non-significance) and data are shown as mean± SD. To normalize the data, each value was divided by the average value of its wild type sibling group, which was set at 100 percent.

Availability of data and materials

Supplementary Movies are available online:
https://www.frontiersin.org/articles/10.3389/fcell.2021.624571/full

3